ELEMENTA
Science of the Anthropocene

Siegel, DA, et al. 2021. An operational overview of the EXport Processes in the Ocean from RemoTe Sensing (EXPORTS) Northeast Pacific field deployment. *Elem Sci Anth*, 9: 1. DOI: https://doi.org/10.1525/elementa.2020.00107

INTRODUCTION

An operational overview of the EXport Processes in the Ocean from RemoTe Sensing (EXPORTS) Northeast Pacific field deployment

David A. Siegel[1,*], Ivona Cetinić[2,3], Jason R. Graff[4], Craig M. Lee[5], Norman Nelson[1], Mary Jane Perry[5,6], Inia Soto Ramos[2,3], Deborah K. Steinberg[7], Ken Buesseler[8], Roberta Hamme[9], Andrea J. Fassbender[10], David Nicholson[8], Melissa M. Omand[11], Marie Robert[12], Andrew Thompson[13], Vinicius Amaral[14], Michael Behrenfeld[4], Claudia Benitez-Nelson[15], Kelsey Bisson[4], Emmanuel Boss[6], Philip W. Boyd[16], Mark Brzezinski[1], Kristen Buck[17], Adrian Burd[18], Shannon Burns[17], Salvatore Caprara[17], Craig Carlson[1], Nicolas Cassar[19], Hilary Close[20], Eric D'Asaro[5], Colleen Durkin[21], Zachary Erickson[22], Margaret L. Estapa[23], Erik Fields[1], James Fox[4], Scott Freeman[2,24], Scott Gifford[25], Weida Gong[26], Deric Gray[27], Lionel Guidi[28], Nils Haëntjens[6], Kim Halsey[4], Yannick Huot[29], Dennis Hansell[20], Bethany Jenkins[11], Lee Karp-Boss[6], Sasha Kramer[1], Phoebe Lam[14], Jong-Mi Lee[14], Amy Maas[30], Olivier Marchal[8], Adrian Marchetti[25], Andrew McDonnell[31], Heather McNair[11], Susanne Menden-Deuer[11], Francoise Morison[11], Alexandria K. Niebergall[19], Uta Passow[32], Brian Popp[33], Geneviève Potvin[29], Laure Resplandy[34], Montserrat Roca-Martí[8], Collin Roesler[35], Tatiana Rynearson[11], Shawnee Traylor[8,36], Alyson Santoro[1], Kanesa Duncan Seraphin[33], Heidi M. Sosik[8], Karen Stamieszkin[7], Brandon Stephens[1], Weiyi Tang[19], Benjamin Van Mooy[8], Yuanheng Xiong[37], and Xiaodong Zhang[38]

[1] University of California, Santa Barbara, Santa Barbara, CA, USA
[2] Ocean Ecology Laboratory, NASA Goddard Spaceflight Center, Greenbelt, MD, USA
[3] GESTAR/Universities Space Research Association, Columbia, MD, USA
[4] Oregon State University, Corvallis, OR, USA
[5] University of Washington, Seattle, WA, USA
[6] School of Marine Sciences, University of Maine, Orono, ME, USA
[7] Virginia Institute of Marine Science, Gloucester Point, VA, USA
[8] Woods Hole Oceanographic Institution, Woods Hole, MA, USA
[9] University of Victoria, Victoria, BC, Canada
[10] National Oceanic and Atmospheric Administration, Pacific Marine Environmental Laboratory, Seattle, WA, USA
[11] University of Rhode Island, Narragansett, RI, USA
[12] Institute of Ocean Science, Sydney, BC, Canada
[13] California Institute of Technology, Pasadena, CA, USA
[14] University of California, Santa Cruz, Santa Cruz, CA, USA
[15] University of South Carolina, Columbia, SC, USA
[16] Institute for Marine and Antarctic Studies, University of Tasmania, Hobart, Australia
[17] University of South Florida, St. Petersburg, FL, USA
[18] University of Georgia, Athens, GA, USA
[19] Nicholas School of the Environment, Duke University, Durham, NC, USA
[20] Rosenstiel School of Marine and Atmospheric Science, University of Miami, Miami, FL, USA
[21] Moss Landing Marine Laboratories, Moss Landing, CA, USA
[22] NASA Postdoctoral Program Fellow, Ocean Ecology Laboratory, NASA Goddard Space Flight Center, Greenbelt, MD, USA
[23] Darling Marine Center, School of Marine Sciences, University of Maine, Walpole, ME, USA
[24] Science Systems and Applications Inc, Lanham, MD, USA
[25] The University of North Carolina at Chapel Hill, Chapel Hill, NC, USA
[26] Lineberger Comprehensive Cancer Center, School of Medicine, University of North Carolina at Chapel Hill, Chapel Hill, NC, USA
[27] Naval Research Laboratory, Washington, DC, USA
[28] Laboratoire d'Océanographie de Villefranche-sur-Mer, Villefranche-sur-Mer, France
[29] Université de Sherbrooke, Sherbrooke, QC, Canada
[30] Bermuda Institute of Ocean Sciences, St. George's, Bermuda
[31] The University of Alaska Fairbanks, Fairbanks, Alaska, USA
[32] Memorial University of Newfoundland, St. John's, NL, Canada
[33] University of Hawaii, Honolulu, HI, USA
[34] Princeton University, Princeton, NJ, USA
[35] Bowdoin College, Brunswick, ME, USA
[36] MIT-WHOI Joint Program in Oceanography, Cambridge, MA, USA
[37] University of North Dakota, Grand Forks, ND, USA
[38] University of Southern Mississippi, Hattiesburg, MI, USA

* Corresponding author:
Email: david.siegel@ucsb.edu

The goal of the EXport Processes in the Ocean from RemoTe Sensing (EXPORTS) field campaign is to develop a predictive understanding of the export, fate, and carbon cycle impacts of global ocean net primary production. To accomplish this goal, observations of export flux pathways, plankton community composition, food web processes, and optical, physical, and biogeochemical (BGC) properties are needed over a range of ecosystem states. Here we introduce the first EXPORTS field deployment to Ocean Station Papa in the Northeast Pacific Ocean during summer of 2018, providing context for other papers in this special collection. The experiment was conducted with two ships: a Process Ship, focused on ecological rates, BGC fluxes, temporal changes in food web, and BGC and optical properties, that followed an instrumented Lagrangian float; and a Survey Ship that sampled BGC and optical properties in spatial patterns around the Process Ship. An array of autonomous underwater assets provided measurements over a range of spatial and temporal scales, and partnering programs and remote sensing observations provided additional observational context. The oceanographic setting was typical of late-summer conditions at Ocean Station Papa: a shallow mixed layer, strong vertical and weak horizontal gradients in hydrographic properties, sluggish sub-inertial currents, elevated macronutrient concentrations and low phytoplankton abundances. Although nutrient concentrations were consistent with previous observations, mixed layer chlorophyll was lower than typically observed, resulting in a deeper euphotic zone. Analyses of surface layer temperature and salinity found three distinct surface water types, allowing for diagnosis of whether observed changes were spatial or temporal. The 2018 EXPORTS field deployment is among the most comprehensive biological pump studies ever conducted. A second deployment to the North Atlantic Ocean occurred in spring 2021, which will be followed by focused work on data synthesis and modeling using the entire EXPORTS data set.

Keywords: Biological pump, NASA field campaign, NPP fates, Carbon cycle, Organic carbon export, Export pathways

Introduction

The biological pump exports roughly 10 Pg of organic carbon from the surface ocean to depth each year (nearly equivalent to the global fossil fuel emission rate), sequestering carbon from the atmosphere and affecting the Earth's climate on time scales of months to millennia (e.g., Boyd et al., 2019; DeVries et al., 2019; Friedlingstein et al., 2019). Through these actions, the biological pump also increases the efficiency of the physical pump to sequester atmospheric CO_2 (e.g., Kwon et al., 2009). The biological pump has three components: sinking flux of particulate organic matter, active transport by daily and seasonally migrating animals, and physical transport due to circulation processes on scales from global meridional overturning to centimeter-scale turbulent motions. Thus, the biological pump is regulated by the coupling of ecological, physiological, behavioral, chemical, particle aggregation, and physical processes, making predicting future states of the biological pump one of the most challenging and, due to its role in the global carbon cycle, most important scientific challenges of our time.

The goal of the EXport Processes in the Ocean from RemoTe Sensing (EXPORTS) field campaign is to develop a predictive understanding of the export and fate of global ocean net primary production (NPP) and its implications for the Earth's carbon cycle in present and future climates (EXPORTS Writing Team, 2015; Siegel et al., 2016). Predicting the carbon cycle impacts of the fate of ocean NPP requires knowledge of (1) the flux of organic matter from the well-lit surface ocean, (2) the vertical attenuation of that downward flux within the ocean interior and its respiration back to dissolved CO_2, and (3) the time scales and paths for these subsurface water masses to ventilate back to the surface. In particular, the vertical transmission of the downward export flux sets the degree to which the biological pump extends into the ocean interior—the deeper this penetration, the longer that organic carbon is sequestered from the atmosphere (e.g., Kwon et al., 2009; Boyd et al., 2019).

The same amount of NPP can lead to very different rates of organic carbon export and vertical flux transmission below the euphotic zone (**Figure 1**; Buesseler and Boyd, 2009; Buesseler et al., 2020b). A comparison of the fraction of NPP that is exported as vertical carbon flux from the euphotic zone (Ez-ratio) with the fraction of that flux that is transmitted to 100 m below the depth of the euphotic zone (T_{100}) clearly reveals that some regions of the global ocean are efficient at exporting NPP and transporting carbon to great depth (high Ez-ratio and T_{100} values), such as the North Atlantic during its spring bloom. Other regions have lower Ez-ratios and T_{100} values, including Ocean Station Papa (Station P) in the subarctic North Pacific (Buesseler and Boyd, 2009, using data collected in 1996 from Charette et al., 1999). The 2018 EXPORTS field campaign results (cross-hatched symbol in **Figure 1**) indicate similar Ez-ratio values to prior observations at Station P but with a higher T_{100}. This difference in T_{100} is thought to be due to the differing definitions of the euphotic zone depths used between studies (see Buesseler et al., 2020a, for further details). Assessing the biological carbon pump over a range of conditions will help ensure that the EXPORTS Field Campaign achieves the predictive understanding we seek, with the Northeast Pacific Ocean EXPORTS field deployment acting as a low efficiency endmember.

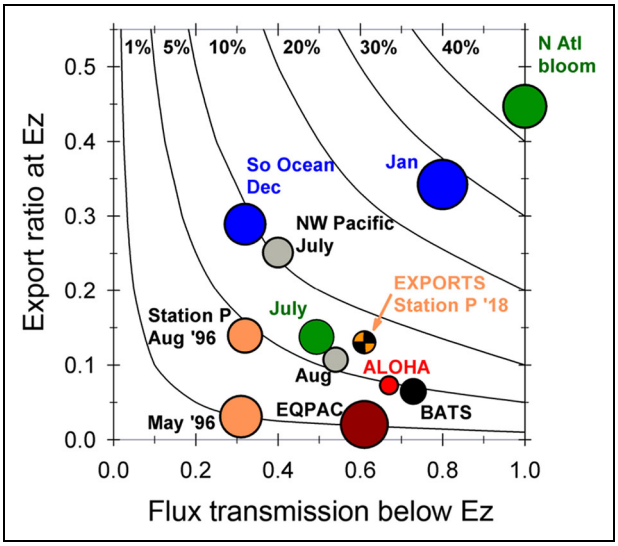

Figure 1. Efficiency of the biological pump measured by export ratio and vertical flux transmission. On the y-axis is the export ratio (Ez-ratio), defined as the fraction of net primary production that is exported as vertical carbon flux from the euphotic zone (Ez); on the x-axis is the fraction of that flux that is transmitted to 100 m below the depth of the euphotic zone (T_{100}). Colors reflect different regional observations of the Ez-ratio and T_{100}: orange are from Station P; green, from the North Atlantic bloom site (N Atl bloom); gray, from the Northwest Subarctic Pacific (NW Pacific); blue, from the Southern Ocean (So Ocean); black, from the Bermuda Atlantic Time Series (BATS); red, from the ALOHA site off Hawaii; and brown, from the Equatorial Pacific (EQPAC). Multiple occurrences of the same region illustrate seasonal differences for these sites. The figure is updated from Buesseler et al. (2020b) to include EXPORTS observations from Station P (orange-black hatched symbol); see text for further details and data sources. DOI: https://doi.org/10.1525/elementa.2020.00107.f1

Three major export pathways link the upper ocean food web with the ocean interior, as depicted in the conceptual "wiring diagram" (**Figure 2**) from the EXPORTS 2015 Science Plan (EXPORTS Writing Team, 2015). These are (1) the gravitational settling of particulate organic matter, which may be composed of intact algal cells, detrital aggregates, and zooplankton byproducts; (2) the active transport of organic carbon to depth by vertically migrating metazoans; and (3) the advective transport of particulate and dissolved organic matter to depth by ocean circulation processes on a myriad of scales. The simultaneous assessment of the export pathways, along with the food web processes that create and alter this organic matter, is a major aim of the EXPORTS field campaign.

The underlying hypothesis for EXPORTS is that the export and carbon cycle fate of ocean NPP can be quantified knowing the characteristics of surface ocean ecosystems, thereby linking biotic carbon cycling processes to ecosystem properties that can be assessed remotely. To test this hypothesis, the EXPORTS Science Plan (Siegel et al., 2016) proposed three fundamental questions:

1. How do upper ocean ecosystem characteristics determine the vertical transfer of organic matter from the well-lit surface ocean?
2. What controls the efficiency of vertical transfer of organic matter below the well-lit surface ocean?
3. How can the knowledge gained from EXPORTS be used to reduce uncertainties in contemporary and future estimates of the export and fate of upper ocean net primary production?

The answers to these questions provide a path toward a predictive understanding of the fates of global ocean NPP and its implications for the Earth's carbon cycle in present and future climates.

EXPORTS builds upon decades of NASA-funded research to develop and validate satellite data-driven models for NPP (e.g., Balch et al., 1992; Behrenfeld and Falkowski, 1997; Campbell et al., 2002; Behrenfeld et al., 2005; Behrenfeld et al., 2006; Behrenfeld et al., 2016; Westberry et al., 2008; Silsbe et al., 2016). EXPORTS will also contribute to NASA's upcoming Plankton, Aerosol, Cloud, ocean Ecosystem mission (e.g., Werdell et al., 2019) by providing a unique data set compiling remote sensing and in situ measurements needed to support biogeochemical (BGC) satellite-based algorithm development and validation.

Here we present the scientific background and programmatic overview of the EXPORTS field campaign and a summary of the oceanographic conditions during the field deployment to Station P to provide context for other papers in this special collection. This introductory paper includes descriptions of campaign logistics, operational timelines, and a comparison of the EXPORTS observations with a climatology for Station P. We also share our plans for the EXPORTS program, as well as ongoing and future analyses of its data.

EXPORTS and the 2018 Northeast Pacific field deployment

A brief history of the EXPORTS field campaign

The history of the EXPORTS field campaign stretches back nearly a decade. The original impetus for EXPORTS came from a scoping project funded by NASA to draft a Science Plan for a large-scale field campaign on the biological pump in 2013. After extensive peer and panel review, the EXPORTS Science Plan was completed (EXPORTS Writing Team, 2015; Siegel et al., 2016). In 2015, NASA formed the EXPORTS Science Definition Team to write an implementation plan that provided guidelines for how the EXPORTS field campaign would be conducted and provided a cost and risk assessment through an ensemble of deployment scenarios (EXPORTS Science Definition Team, 2016). The EXPORTS implementation plan called for a multi-scale

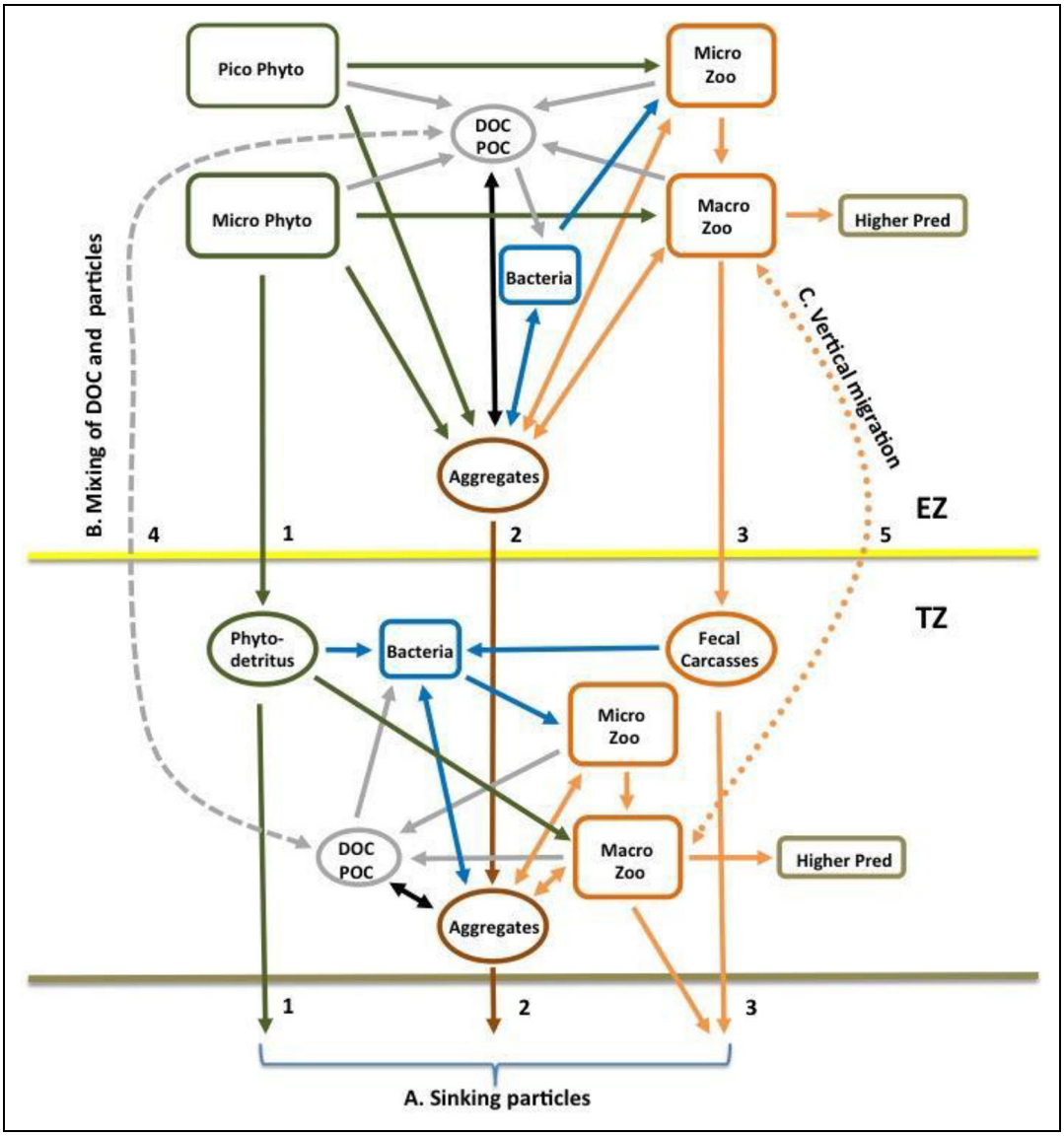

Figure 2. Conceptual food web diagram from the EXPORTS Science Plan. Shown here is the conceptual food web diagram or "wiring diagram" from the EXPORTS Science Plan (EXPORTS Writing Team, 2015). The upper portion represents the euphotic zone (EZ) food web while the lower portion represents the mesopelagic zone, sometimes referred to as the twilight zone (TZ). These two regions are connected via the vertical flux pathways due to (A) sinking particles, (B) physical mixing of particles and dissolved organic carbon (DOC), and (C) the vertical migration of macrozooplankton and higher trophic organisms. The EZ food web denotes the input of net primary production by picophytoplankton and microplankton, the grazing by microzooplankton and microzooplankton and the recycling of some of the NPP energy by the microbial loop. Sinking particles can leave the EZ via (1) phytodetritus, (2) aggregates, and (3) fecal materials and zooplankton carcasses. The TZ food web consumes and recycles organic matter transferred to it via the three major pathways. The organic carbon consumption within the TZ food web controls the transmission of the sinking particle flux to depth. DOI: https://doi.org/10.1525/elementa.2020.00107.f2

sampling approach, combining two ships and autonomous underwater vehicles (AUVs) leveraging ongoing partnership programs, as depicted in **Figure 3**.

NASA structured the EXPORTS field campaign as a multiyear effort with a "Pre-EXPORTS" modeling and data-mining activity followed by a first phase with two major field programs and a second synthesis and modeling phase (**Figure 4**). The "Pre-EXPORTS" projects helped to plan the field campaign (e.g., Rousseaux and Gregg, 2017; Resplandy et al., 2019) and to create data sets mined from the literature (e.g., Bisson et al., 2018; Bisson et al., 2020; Kramer and Siegel, 2019) that can be useful for global syntheses (**Table 1**). These efforts were followed by Phase 1 of EXPORTS, where the Science Team openly competed to conduct field deployments in the Northeast Pacific in late summer 2018 and in the North Atlantic in spring 2020. Several individual projects also received support from the U.S. National Science Foundation (NSF), with all NSF principal investigators joining the EXPORTS Science Team (**Table 1**). The objectives of Phase 1 are to collect the

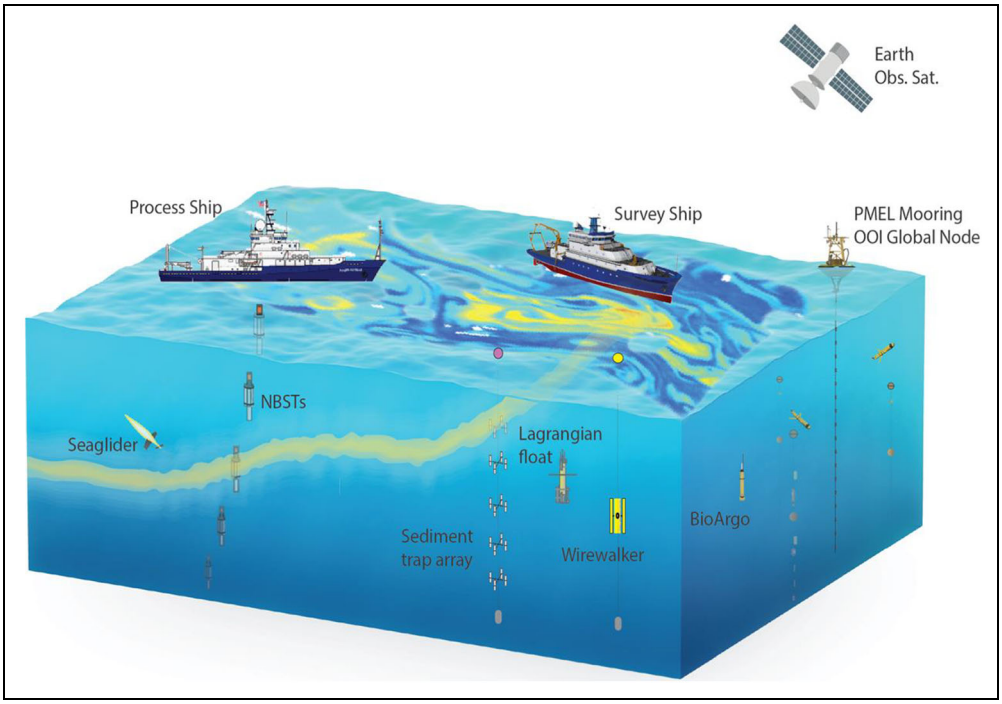

Figure 3. Conceptual diagram of the sampling array for the EXPORTS Northeast Pacific Field Deployment. The sampling array for the EXPORTS Northeast Pacific field deployment is composed of both ship and autonomous sampling platforms. Two ships were deployed: a Process Ship, the R/V *Roger Revelle*; and a Survey Ship, the R/V *Sally Ride*. The autonomous sampling array was highly heterogeneous with an instrumented Lagrangian float that the Process Ship followed, a Seaglider, multiple neutrally buoyant sediment traps (NBSTs), a surface-tethered sediment trap array, an instrumented Wirewalker profiler, and two biogeochemical Argo profilers. The EXPORTS Northeast Pacific field deployment was conducted at Station P in the Northeast Pacific (near 45°N 145°W) which is a Global Node of the U.S. NSF's Ocean Observatories Initiative (OOI). DOI: https://doi.org/10.1525/elementa.2020.00107.f3

necessary data to answer science questions 1 and 2, submit collected data to national repositories (SeaBASS and BCO-DMO) making them publicly available for all interested users, and conduct preliminary syntheses and modeling.

Following conclusion of the field components of Phase 1 and submission of collected data to public repositories, NASA plans to solicit proposals for the Phase 2 synthesis and modeling effort with a focus on further synthesis of the field results from Phase 1 and their application to improve global models of carbon cycle impacts of NPP fates. In March 2020, the COVID-19 pandemic led to the decision to postpone the North Atlantic deployment until the spring of 2021.

Site selection and its oceanographic characteristics

The EXPORTS NE Pacific deployment was conducted at Ocean Station Papa (Station P, nominally 50° N, 145° W). Station P is among the most well-studied open-ocean sites in the world (e.g., Tabata, 1965; Davis et al., 1981; Miller et al., 1991; D'Asaro et al., 1995; Wong et al. 1995; Boyd et al., 1999; Boyd et al., 2004; Whitney et al., 2005). In the 1940s, Ocean Weather Station Papa was established to provide weather information for forecasting. The first oceanographic samples were collected in 1949 by U.S. vessels, and standard hydrographic sampling commenced in 1956 by Canadian vessels and personnel (Freeland, 2007). Today, Station P is the terminus of Canada's Line P time-series sampling program, constituting one of the longest ongoing oceanographic time series, and is the site of instrumentation from the U.S. Ocean Observing Initiative (OOI), University of Washington Applied Physics Lab (UW-APL) waverider moorings, and the NOAA Pacific Marine Environmental Laboratory (NOAA-PMEL) air-sea interaction mooring (see **Figure 5** for a map illustrating the locations of these moored assets, as well as the EXPORTS ship tracks). The Canadian Line P program reoccupied the EXPORTS site roughly 10 days after the EXPORTS ships left the Station P site.

Upper ocean stratification at Station P during the summer can be characterized by three main features: a mixed layer, thermocline, and halocline (**Figure 6**). The mixed layer typically extends between 20 and 30 m in the summer and deepens to roughly 100 m in winter. During the summer months, the mixed layer overlies a shallow seasonal thermocline that sits at the base of the mixed layer, whereas the wintertime mixed layer depth (MLD) marks the top of a seasonal pycnocline that is dominated by salinity stratification, the halocline. The temperature in the mixed layer undergoes a large seasonal cycle, peaking around 12 °C to 14 °C in the summer and cooling to 5 °C to 6 °C in the winter (**Figure 7**). The surface salinity shows smaller temporal variability spanning 32.4–32.6 in the surface layer with a larger variation of 0.6 in the thermocline layer (Pelland et al., 2017).

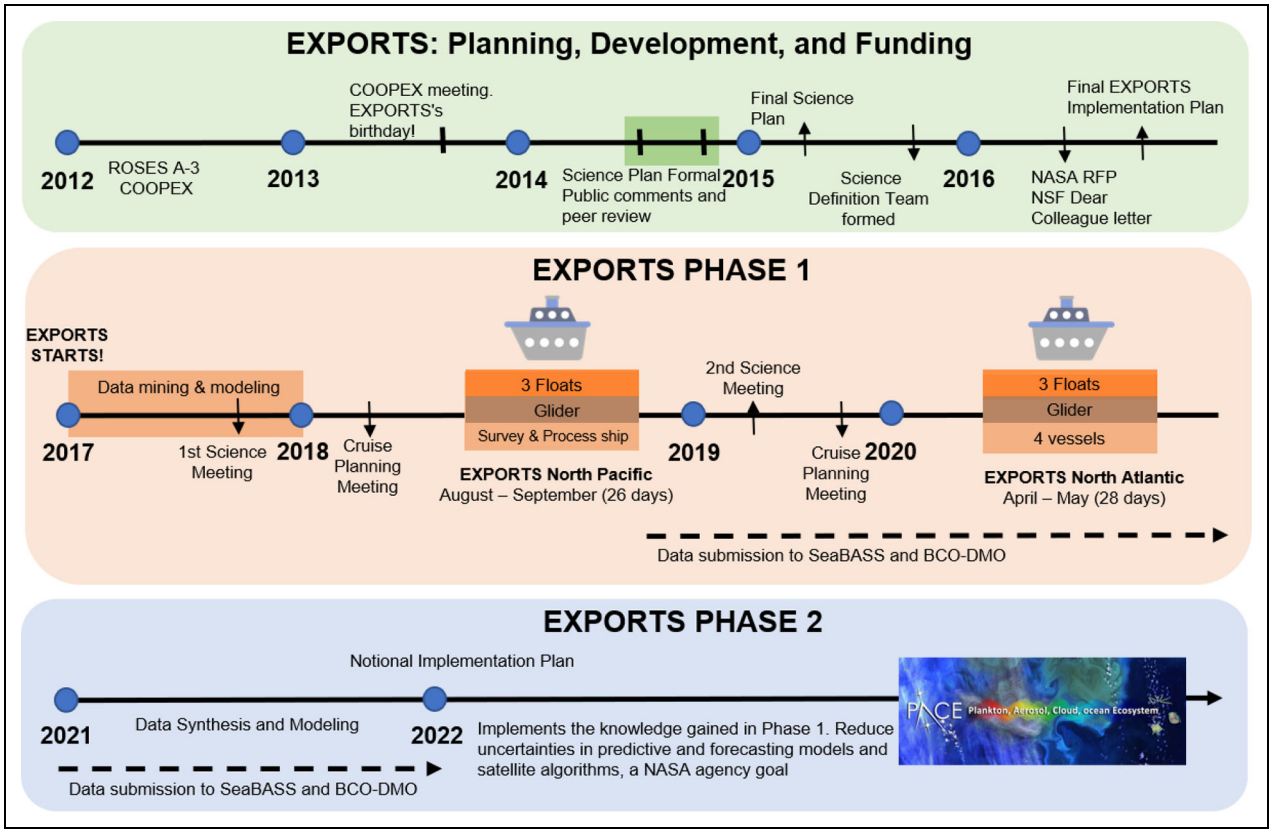

Figure 4. Timeline for the NASA EXPORTS Field Campaign. Shown here is the original NASA time line for the EXPORTS Field Campaign before postponement of the 2020 North Atlantic cruise due to the COVID-19 pandemic. The three boxes arranged vertically illustrate the planning, development and funding period (upper green), the Phase 1 field program (middle tan), and the planned Phase 2 data synthesis and modeling program (bottom blue). The NE Pacific cruise, the subject of this special collection of *Elementa*, is the first major field deployment for the Phase 1 program. The second field deployment to the North Atlantic was postponed due to the COVID-19 pandemic, but is underway at the time of manuscript acceptance (May 2021). The postponement of the second field deployment also pushes the start date for the Phase 2 program forward by at least a year. DOI: https://doi.org/10.1525/elementa.2020.00107.f4

The low-frequency circulation at Station P is dominated by the North Pacific Current, a slow, eastward-flowing current that separates the North Pacific Subtropical and Subpolar Gyres (e.g., Cummins and Freeland, 2007). Over shorter time scales, the one-dimensional balances described above can be disrupted by other processes that include spatial shifts in the North Pacific Current or the rare passage of mesoscale eddies (Freeland and Cummins, 2005; Jackson et al., 2006; Pelland et al., 2016). Eddy kinetic energy in the northeastern Pacific Ocean is among the lowest in the global ocean (e.g., Chelton et al., 2007; Xu et al., 2014), and coherent mesoscale circulation features are rarely seen, as Station P is noted to be an "eddy desert" (e.g., Chelton et al., 2011). In contrast, instantaneous currents are dominated by near-inertial wave motions due to the relatively strong wind forcing shallow mixed layers and weak mean and mesoscale currents at this site (e.g., D'Asaro et al., 1995). The dominance and relatively large horizontal scales of near-inertial motions makes Station P, in many regards, an ideal location to test one-dimensional models of mixed layer evolution (e.g., Denman and Miyake, 1973; Mellor and Durbin, 1975; Large et al., 1994).

Station P is also located in one of the three major iron-limited, high-nutrient, low-chlorophyll (HNLC) regions of the world ocean. Low iron availability limits phytoplankton production and thereby surface chlorophyll (*Chl a*) concentrations (e.g., Boyd et al., 2004). Previous to John Martin's demonstration of iron limitation in this area (Martin and Fitzwater, 1988), primary productivity was assumed to be limited by light and phytoplankton biomass to be kept low by zooplankton grazing (Parsons and Lalli, 1988). Martin's finding of iron limitation was at first controversial. However, shipboard carboy experiments at Station P validated that iron controlled primary productivity in late spring and summer (Boyd et al., 1996) and that mesozooplankton grazing could not fully consume the increased phytoplankton biomass when iron was added in carboys (Boyd et al., 1999). The in-situ SERIES iron enrichment experiment conducted in July of 2002 further verified iron limitation through the induction of a large phytoplankton bloom, composed primarily of diatoms, following iron enrichment (Boyd et al., 2004). Climatological surface nitrate concentrations are consistently in excess of 9 μmol L^{-1} throughout the region surrounding Station P (**Figure 5**; Whitney and Freeland, 1999), and

Table 1. EXPORTS science team. DOI: https://doi.org/10.1525/elementa.2020.00107.t1

Principal Investigators (Affiliation)	Project Title	Funding Agency
Behrenfeld[a] (Oregon State University, OSU), Boss (University of Maine, UMaine), Graff (OSU), Guidi (Laboratoire d'Océanographie de Villefranche, LOV), Halsey (OSU), Karp-Boss (UMaine)	First step—Linking remotely detectable optical signals, photic layer plankton properties, and export flux	NASA ST[b]
Buesseler (Woods Hole Oceanographic Institution, WHOI), Benitez-Nelson (University of South Carolina), Resplandy (Princeton)	Elucidating spatial and temporal variability in the export and attenuation of ocean primary production using Thorium-234	NASA ST
Carlson (University of California, Santa Barbara, UCSB), Hansell (University of Miami, UMiami)	Evaluating the controls of dissolved organic matter accumulation, its availability to bacterioplankton, its subsequent diagenetic alteration and contribution to export flux	NASA ST
Close (UMiami), Popp (University of Hawaii, UH), Seraphin (UH)	Isotopic indicators for mechanisms of organic matter degradation in the Northeast Pacific	NSF
Churnside (NOAA)	Lidar data mining in support of EXPORTS	NASA Pre
Estapa (Skidmore College, UMaine[c]), Buesseler (WHOI), Durkin (Moss Landing Marine Laboratories), Omand (University of Rhode Island, URI)	Linking sinking particle chemistry and biology with changes in the magnitude and efficiency of carbon export into the deep ocean	NASA ST
Fassbender (Monterey Bay Aquarium Research Institute, NOAA PMEL[c])	Constraining upper ocean carbon export with biogeochemical profiling floats	NSF
Jenkins (URI), Buck (University of South Florida), Brzezinski (UCSB)	Diatoms, food webs and carbon export—leveraging NASA EXPORTS to test the role of diatom physiology in the biological carbon pump	NSF
Lam (University of California Santa Cruz, UCSC), Marchal (WHOI), Lee (UCSC)	Collaborative research: Estimation of particle aggregation and disaggregation rates from the inversion of chemical tracer data	NSF
Lee (University of Washington, UW), D'Asaro (UW), Nicholson (WHOI), Omand (URI), Perry (UMaine), Thompson (CalTech)	Autonomous investigation of export pathways from hours to seasons	NASA ST
Mahadevan (WHOI), Nicholson (WHOI), Omand (URI)	Modeling studies for EXPORTS in a dynamic ocean environment	NASA Pre
Marchetti (University of North Carolina, UNC), Cassar (Duke), Gifford (UNC)	Quantifying the carbon export potential of the Marine microbial community: Coupling of biogenic rates and fluxes with genomics at the ocean surface	NASA ST
McGillicuddy (WHOI), Lévy (Laboratoire d'Océanologie et de Climatologie), Resplandy (Princeton)	Mechanisms controlling mesoscale/submesoscale hotspots in net community production/export, with simulation-based studies on how to sample them	NASA Pre
Menden-Deuer (URI), Rynearson (URI)	Quantifying plankton predation rates, and effects on primary production, phytoplankton community composition, size spectra and potential for export	NASA ST
Roesler (Bowdoin College), Sosik (WHOI)	Phytoplankton community structure, carbon stock, carbon export and carbon flux: What role do diatoms play in the North Pacific and North Atlantic Oceans?	NASA ST
Rousseaux (USRA/NASA GSFC), Cetinić (USRA/NASA GSFC), Gregg (NASA GSFC), Romanou (NASA GISS)	Observation-system simulation experiments (OSSEs) and seasonal forecasts to support EXPORTS	NASA Pre
Santoro (UCSB), Boyd (University of Tasmania)	Surface vs. subsurface controls on microbial attenuation of sinking particulate flux in the Mesopelagic Ocean	NASA ST
Siegel (UCSB), Buesseler (WHOI)	Data mining global ocean ecosystem and carbon cycling observations for EXPORTS planning and synthesis	NASA Pre

(continued)

TABLE 1. *(continued)*

Principal Investigators (Affiliation)	Project Title	Funding Agency
Siegel (UCSB), Burd (University of Georgia), McDonnell (University of Alaska - Fairbanks), Nelson (UCSB), Passow (Memorial University of Newfoundland)	Synthesizing optically and carbon export–relevant particle size distributions for the EXPORTS field campaign	NASA ST
Steinberg (Virginia Institute of Marine Science), Maas (Bermuda Institute for Ocean Sciences)	Zooplankton-mediated export pathways: Quantifying fecal pellet export and active transport by diel and ontogenetic vertical migration in the North Pacific and Atlantic Oceans	NASA ST
Van Mooy (WHOI)	Environmental lipidomics of suspended and sinking particles in the upper ocean	NSF
Zhang (University of South Mississippi), Gray (Naval Research Laboratories), Guidi (LOV), Huot (Université de Sherbrooke)	Optically resolving size and composition distributions of particles in the dissolved-particulate continuum from 20 nm to 20 mm to improve the estimate of carbon flux	NASA ST

[a]Lead PIs underlined.

[b]ST indicates science team; Pre indicates modeling and data mining activities prior to EXPORTS Phase 1.

[c]Denotes current affiliation.

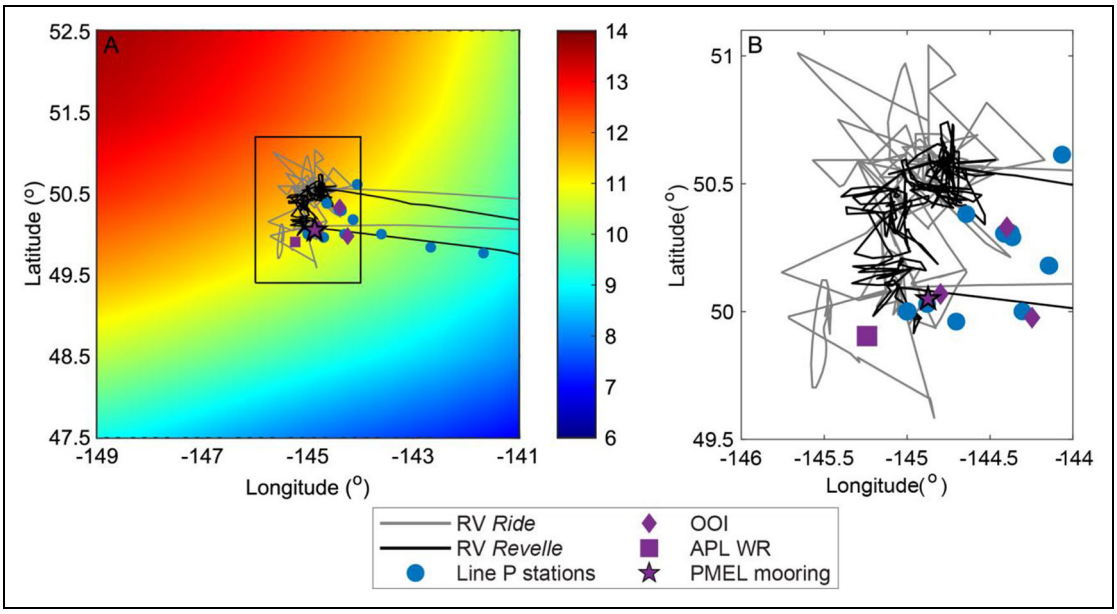

Figure 5. Site map for the EXPORTS Northeast Pacific field deployment. (A) Annual mean surface nitrate concentrations (color bar in µmol kg^{-1}) from the 2013 World Ocean Atlas (https://www.nodc.noaa.gov/OC5/woa13/) along with ship tracks of the R/V *Revelle* (black line) and R/V *Ride* (gray line) in the boxed area, and Canadian Line P stations from their Fall 2018 cruise (Line P cruise 2018-40; blue circles). (B) Enlargement of inset in (A) showing locations of the NOAA PMEL air-sea interaction mooring (purple star), UW-APL waverider buoy (purple square), and NSF OOI subsurface moorings (purple diamonds) along with locations of proximal Line P stations from their Fall 2018 cruise (Line P cruise 2018-40; https://www.waterproperties.ca/linep/2018-040/; blue circles), as well as ship tracks of the R/V *Revelle* (black line) and R/V *Ride* (gray line). DOI: https://doi.org/10.1525/elementa.2020.00107.f5

dissolved Fe concentrations in these surface waters are typically less than 10 pM (Martin et al., 1989; Schallenberg et al., 2017). Thus, special care is required to ensure that seawater for trace metal composition and biological rate measurements are collected and processed using trace metal clean (TMC) techniques, as was done during the 2018 EXPORTS cruise.

Temperature and salinity profiles from recent late-August cruises at Station P show a shallow well-mixed surface layer, a strong seasonal thermocline from roughly 30–60 m, and a strong stratifying halocline between roughly 100 and 130 m which defines the permanent pycnocline at this site (**Figure 6A** and **B**). In August, the mean ($\pm$standard deviation) MLD is 23 $\pm$ 8 m (using

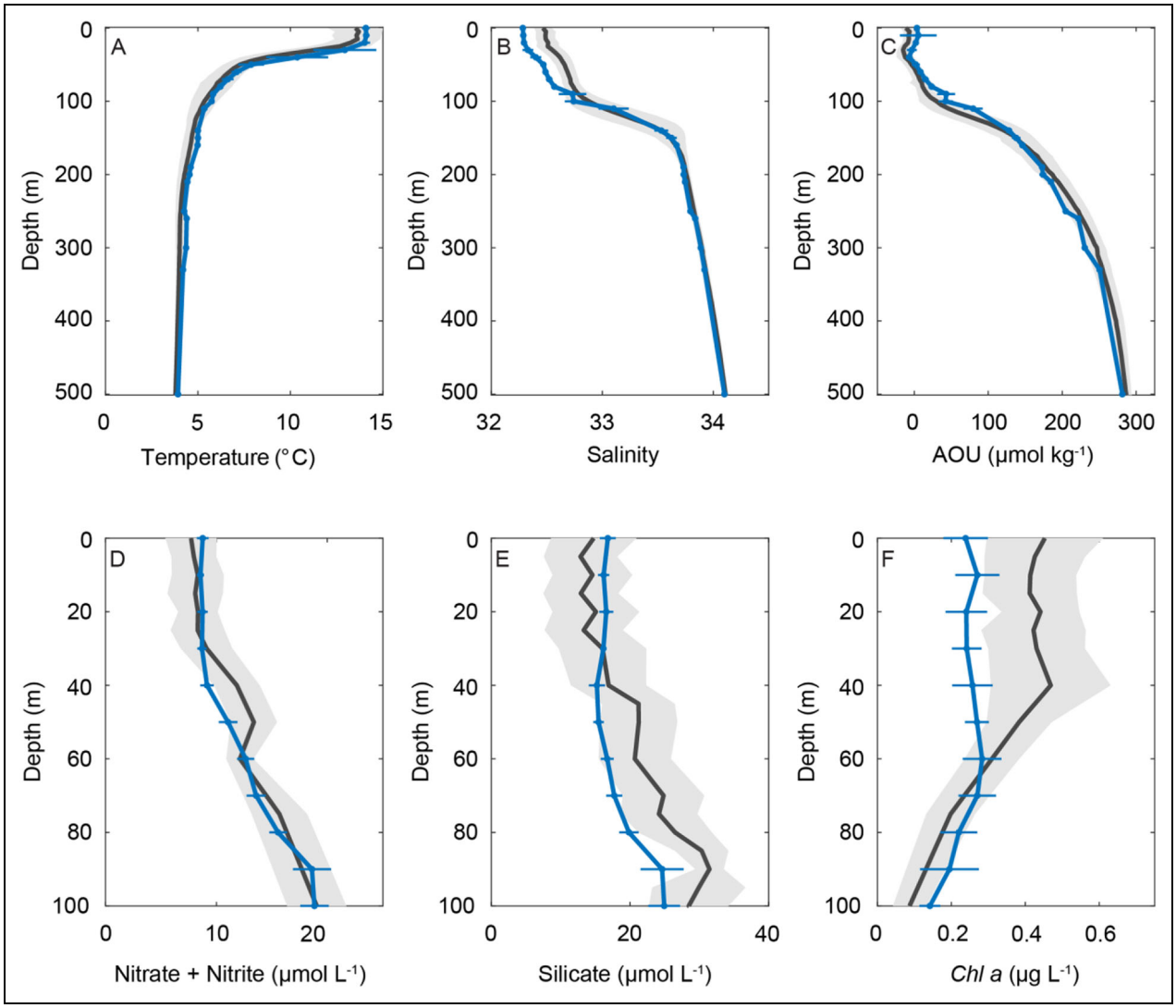

Figure 6. Comparison of Line P Station P26 August climatology (2000–2017) and EXPORTS observations (2018). Mean climatological values for Canadian Line P station P26 from August cruises for the years 2007–2016 are depicted as black lines (with gray 95% confidence interval envelopes about the mean). In blue are mean values (with 95% confidence interval envelopes) collected during EXPORTS 2018 (from Process Ship). Profiles shown are for (A) temperature, (B) salinity, (C) apparent oxygen utilization, (D) nitrate + nitrite, (E) silicate, and (F) *Chl a* (fluorometric). A–C are from rosette-mounted sensor data; D–F are from samples collected from Niskin bottles. DOI: https://doi.org/10.1525/elementa.2020.00107.f6

a 0.2 °C criteria; $n = 10$) when evaluated over the 10-year subset of Line P data, while the mean MLD during EXPORTS using the same criteria was 29 $\pm$ 4 m ($n = 226$). The maximum observed MLD from Line P station P26 within the period from 2007 to 2017 is about 120 m during February, consistent with the depth of the permanent pycnocline. Temperature and salinity profiles during the EXPORTS campaign are very similar in shape with the August mean at Line P Station P26, although the upper 90 m of the water column during EXPORTS was significantly fresher than the climatology. Apparent oxygen utilization (AOU) values are saturated in the upper 90 m of the water column and supersaturated (AOU < 0 µmol kg^{-1}) just beneath the mixed layer (**Figure 6C**) in both data sets. Values of AOU increase to nearly 300 µmol kg^{-1} at 500 m, illustrating the depletion of dissolved oxygen concentrations at depth due to remineralization (e.g., Bushinsky and Emerson, 2015; Pelland et al., 2018).

Nitrate (+ nitrite) concentrations from Line P station P26 are roughly 8 µmol L^{-1} in the mixed layer and increase to approximately 18 µmol L^{-1} at 500 m (**Figure 6D**). Line P silicate concentrations are roughly 15 µmol L^{-1} in the upper layers and increase to nearly 30 µmol L^{-1} at a depth of 100 m. Concentrations of both nutrients found during EXPORTS follow these general patterns (**Figure 6D** and **E**). Mixed layer *Chl a* concentrations observed during EXPORTS (0.25 µg L^{-1}), however, were lower than the Line P average (0.45 µg L^{-1}, **Figure 6E**). The nutrient and relatively low *Chl a* concentrations observed support the characterization of Station P as an HNLC site.

For August, the average fractional isolume depths for photosynthetically available radiation (PAR) fluxes from

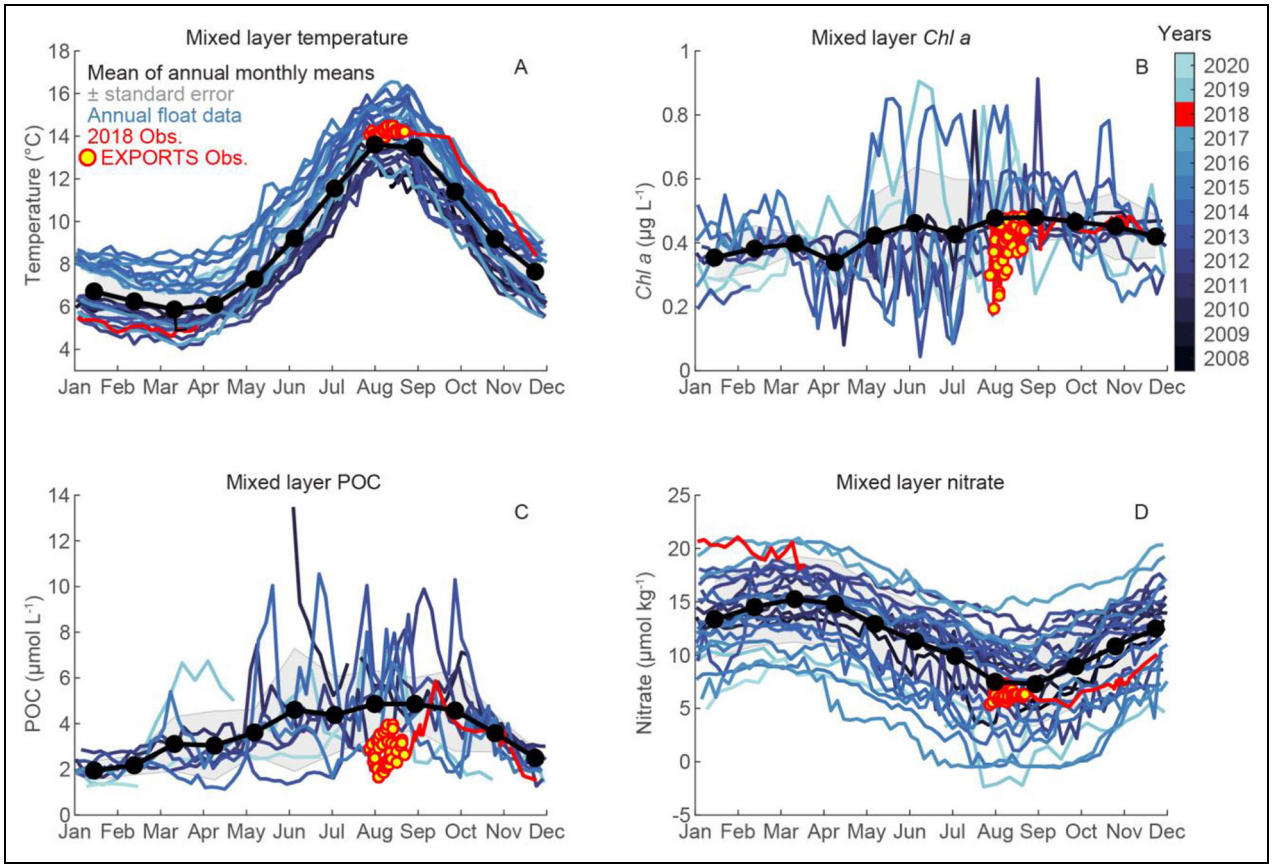

Figure 7. Climatology of mixed layer properties from historical BGC float records near Station P. Mixed layer averages are shown for (A) temperature, (B) *Chl a*, (C) particulate organic carbon, and (D) nitrate. The thick black line with filled circles is the respective monthly climatology calculated as the average of the monthly means for the years 2008–2020, and the shaded gray envelope represents the associated standard error. Individual yearly records are denoted in the color bar; observations from 2018 and the EXPORTS campaign are shown by the red line and with yellow-filled red circles, respectively. DOI: https://doi.org/10.1525/elementa.2020.00107.f7

Line P station P26 were 55 ± 10 m (as standard deviation, $n = 10$) for the 1% PAR isolume and 95 ± 11 m ($n = 10$) for the 0.1% PAR isolume depth. During EXPORTS, depths of the 1% PAR isolume ranged from 70 to 90 m with a mean of 78 ± 6 m ($n = 149$). These deeper fractional isolume depths reflect the lower *Chl a* concentrations observed during EXPORTS compared with typical Line P observations for the period from 2007 to 2017.

Since 2008, a series of BGC profiling floats have collected data on the physical and biological properties of the water column in the vicinity of Station P (**Figure 7**; Bushinsky and Emerson, 2015; Plant et al., 2016; Yang et al., 2018; Bif et al., 2019; Haskell et al., 2020). Mixed layer temperatures change on average by 6 °C to 9 °C from winter to summer, with the EXPORTS cruise happening during the warmest time of the year. Mixed layer mean concentrations of *Chl a* and particulate organic carbon tend to increase from winter through a peak in late summer with a considerable amount of interannual variation about these trends. BGC float-sensed nitrate concentrations typically decrease from March through September by about 7 µmol kg^{-1}, again with considerable interannual variability. BGC float observations during EXPORTS (**Figure 7**) occurred in slightly warmer mixed layer temperatures and lower POC, *Chl a*, and nitrate concentrations.

Operational details for the 2018 EXPORTS Northeast Pacific field deployment

The EXPORTS 2018 field deployment consisted of four major components (depicted in **Figures 3** and **8** and listed in **Table 2**). First, the R/V *Roger Revelle* functioned as the Process Ship, sampling BGC stocks and fluxes, ecological abundances and rates, and optical properties following a Lagrangian float. Second, the R/V *Sally Ride* was the Survey Ship and characterized spatial variability about the Process Ship on scales from about 1 to 100 km. Third, a heterogeneous array of AUV platforms was deployed to set the spatial center of the sampling program, to provide horizontal spatial and high-temporal information, and to extend the temporal presence in the area. Last, a long-term sampling presence was created, tying the ship-based observations to climatically relevant time and space scales using BGC floats and partnerships with ongoing research programs.

The mission of the Process Ship, the R/V *Revelle*, was to constrain the pathways for organic carbon transformation and export, sampling in three distinct 8-day sampling

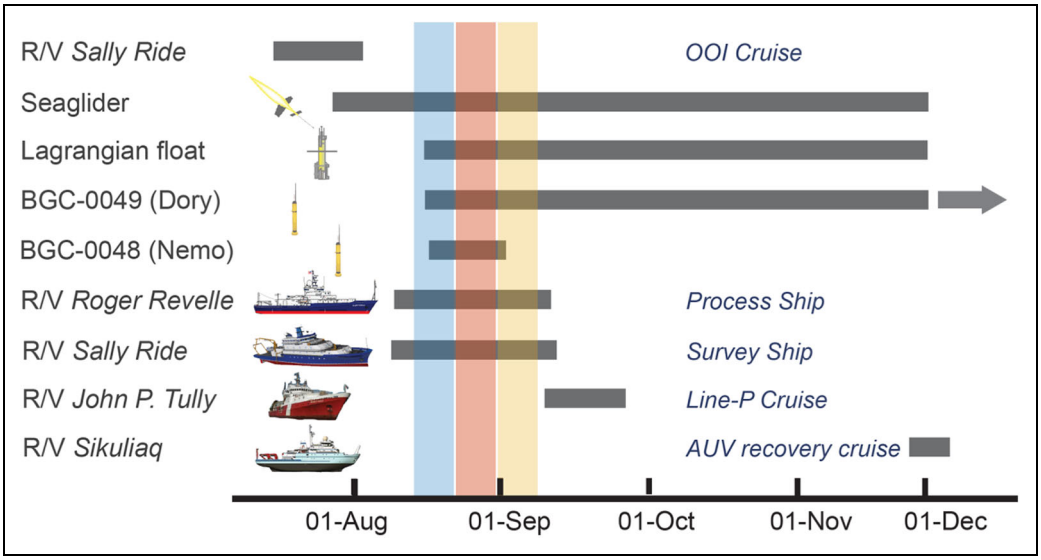

Figure 8. Experimental timeline for the 2018 EXPORTS Northeast Pacific field deployment. Colored vertical bars indicate the three sampling cycles or "epochs" of the 2018 EXPORTS field campaign, while gray horizontal bars indicate deployment periods for each of the platforms. Note that one of the biogeochemical floats (BGC-0049) was still operational at the time of submission of this manuscript. DOI: https://doi.org/10.1525/elementa.2020.00107.f8

cycles or epochs. The length of the epochs was set by the goal of sampling the same particles that are generated during the epoch as well as the operational reality of conducting the export pathway measurements. This sampling plan required the deployment of standard and trace-metal-clean CTD/rosette systems for collection of water samples and physical and BCG sensor data. A customized underway flow-through system allowed for continuous analysis of phytoplankton, particles, dissolved constituents, net community production, and optics from near-surface seawater (**Table 2**). Operations also included the deployment of a multiple opening/closing net (MOCNESS) for assessing depth-discrete day–night differences in zooplankton populations, neutrally buoyant sediment traps (NBSTs), a surface-tethered sediment trap array (STT) that included in situ respiration traps, marine snow catchers for collecting sinking particles and assessing their fluxes, a Wirewalker (WW) for high resolution profiling of physical and bio-optical properties, a TMC towfish, and in situ and underway above-water bio-optics (**Table 2**). Plankton and microbial community structure were measured using a variety of techniques, including classical microscopy, flow cytometry, high-throughput microscopic imaging systems, metacommunity genomic sequencing, and gel trap-collected sinking particles. Phytoplankton rate measurements were made using TMC sampling methods (e.g., Measures et al., 2008; Mellet and Buck, 2020) with flow-through deckboard incubators screened for in situ light levels, with some incubators chilled to match the temperature below the mixed layer (including microzooplankton grazing, and mesozooplankton fecal pellet production rates). Additional rates were measured in temperature- and light-controlled laboratory incubators (e.g., bacterial production, microbial and zooplankton respiration, and particle sinking velocity).

Operations were conducted in three consecutive sampling cycles or "epochs" of 8-day duration (**Figure 9A**). Each epoch began with a positioning of the ship proximate to the Lagrangian float (LF) and deployment of the WW and surface-tethered sediment traps on day 1. NBSTs were subsequently deployed, with staggered recovery (3–5 days later) dependent on collection depth (**Figure 9A**). Shallow (0–150 m) predawn CTD casts (including TMC casts) every other day were used for primary production measurements conducted in deckboard incubators, and deeper (0–1,000 m) casts for multiple measurements occurred mid-day each day, and at night (for diel plankton composition and other comparisons) about every other day. A pair of day/night MOCNESS tows, centered on local noon and midnight, occurred on Days 2 and 7, with other net tows for live zooplankton experiments interspersed. Optics casts centered on the noon hour and occurred on most days, weather permitting. Marine snow catcher deployments and subsequent settling times occurred four days per epoch, which was also the maximum deployment time for the TMC towfish (**Figure 9A**). The spatial map (**Figure 9B**) illustrates the ship's track with trajectories of the sediment traps (NBST and STT) and WW deployed in the three epochs superimposed. Typically, NBSTs drifted 5–25 km depending on their deployment depth. Each day the ship embarked on a "poop run" to dump sewage holding tanks outside of a circle of 10-km radius extending from in-water assets (particularly sediment traps). These excursions can be seen in the ship tracks as large excursions from the central trajectory of the ship (**Figure 9B**) and proved useful to supplement spatial sampling from the ship's underway system.

The second component was the Survey Ship, the R/V *Sally Ride*. Its mission was to characterize the horizontal and vertical distribution of properties including phytoplankton, particulate and dissolved organic carbon,

Table 2. EXPORTS sampling platforms and measurements. DOI: https://doi.org/10.1525/elementa.2020.00107.t2

Platform	Sampling System	Types of Measurements Made
Process Ship R/V *Revelle*	CTD/Rosette	CTD and bio-optical sensors, large particle imaging (UVP-5) and small particle size distribution (LISST-Deep) profiles, Niskin water samples for further analyses
	Underway	CTD and bio-optical sensors, hyperspectral absorption/attenuation, multispectral backscatter, fast repetition rate fluorometry, small particle imaging (Imaging Flow Cytobot [IFCB]), net community production (O_2/Ar) time series at 5-m intake depth with discrete samples
	TMC CTD/ Rosette	Trace metal clean (TMC) collection of discrete water samples with CTD sensors
	TMC towfish	Large volume TMC collection of water for experiments
	MOCNESS	Multiple opening/closing net and environmental sensing system (MOCNESS) that enables zooplankton collections in depth-discrete intervals from 0 to 1,000 m with CTD sensors
	Net tows	Vertically integrated collection of live zooplankton for experimental work
	Marine snow catchers	Large volume (100 L) sampling bottles that enable particles to be sorted based upon sinking speeds
	Sediment traps	Neutrally buoyant and surface-tethered sediment trap arrays with polyacrylamide gel, O_2 respiration and optical sediment traps, upward looking cameras
	Wirewalker	Hourly profiles of CTD and bio-optical sensor data to about 500 m
	In situ optics	Compact optical profiling system (C-OPS) spectroradiometer profiles, near-surface hyperspectral reflectance (THSRB), slow-drop inherent optical property (IOP) profiling system and multispectral backscatter
	Above water optics	Hyperspectral ocean reflectance from bow-mounted system (HyperSAS)
Survey Ship R/V *Ride*	CTD/Rosette	CTD and bio-optical sensors, large particle imaging (UVP-5) and small particle size distribution (LISST-Deep) profiles and in situ NO_3 concentration profiles, Niskin samples for further analyses
	Underway	CTD and bio-optical sensors, hyperspectral absorption/attenuation, multispectral backscatter, small particle imaging (IFCB), net community production (O_2/Ar), pH and NO_3 time series at 5 m intake depth with discrete samples
	Large volume pumps	Size-fractionated, large volume particle sampling at 6 depths
	In situ optics	C-OPS spectroradiometer profiles, THSRB hyperspectral reflectance spectra and lowering frame with hyperspectral absorption/attenuation, multispectral backscatter, small particle size distribution profiles
	Above water optics	HyperSAS ocean reflectance from bow-mounted system
Autonomous vehicles	Lagrangian float	Followed flow at about 100 m, instrumented with CTD, O_2, optical backscatter, chlorophyll fluorescence and NO_3 sensors; profiles made daily when ships were out, every other day before and after; operational Aug–Dec 2018
	SeaGlider	Sampling from the surface to about 1,000 m around the Lagrangian float and ships, profiles every 6 h, instrumented with CTD, O_2, optical backscatter, chlorophyll fluorescence, spectral downwelling irradiance (412, 443, 554 nm, PAR) and acoustic Doppler current profiler sensors; operational July–December 2018
	BGC float	Profiling floats to about 2,000 m; burst sampling of 3 profiles in 24 h, every 3 d during EXPORTS campaign, profiling at 10-d interval afterwards; instrumented with CTD and bio-optical, NO_3, pH, and O_2 sensors; operational Aug 2018-present (BGC-0049) and August–September 2018 (BGC-0048)
	Wirewalker	Profiles every 40 min from surface to about 500 m, instrumented with CTD and O_2, optical backscatter, chlorophyll fluorescence, CDOM fluorescence, beam attenuation and PAR sensors; deployed at the start and recovered at the end of every epoch

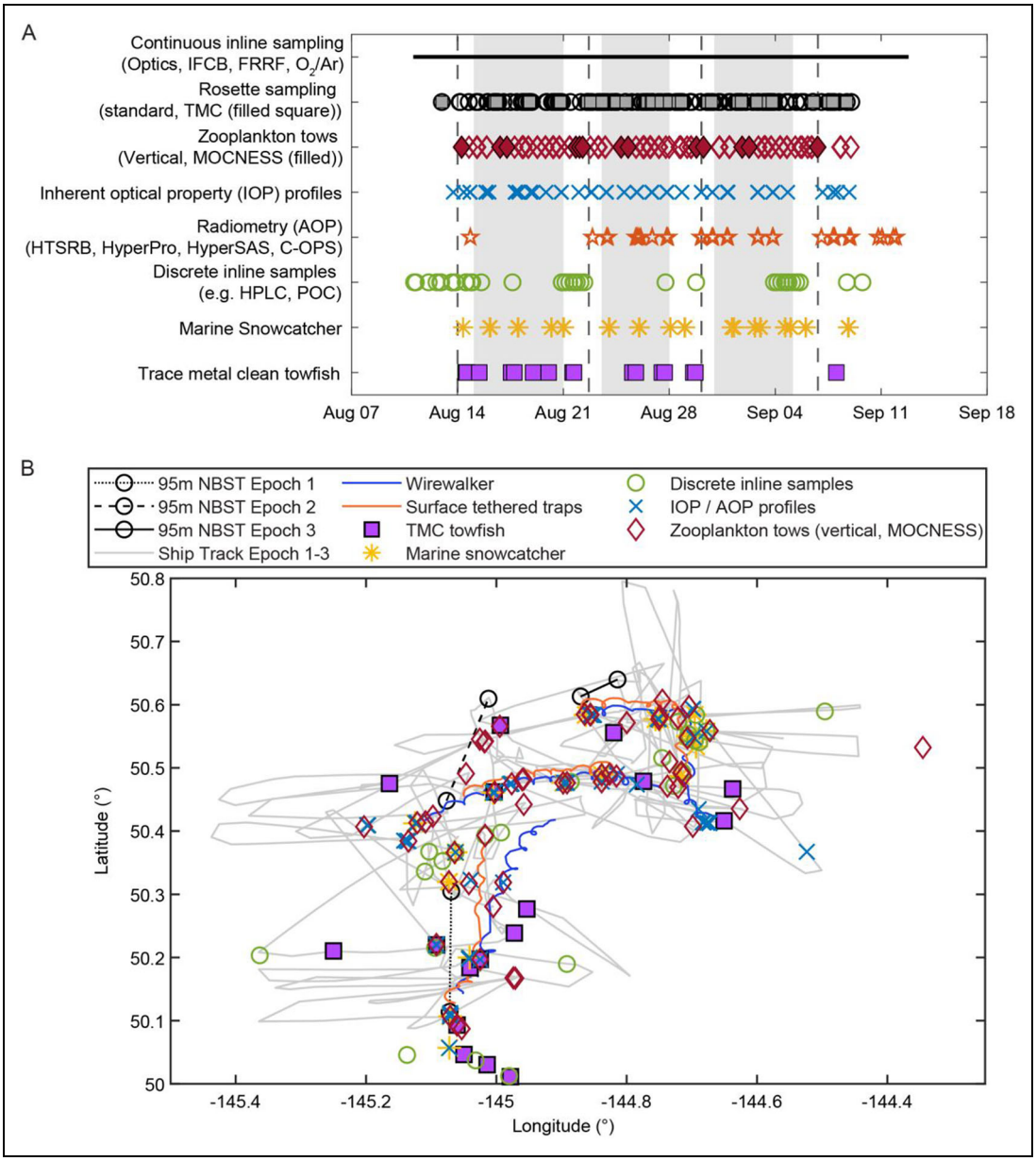

Figure 9. Temporal and spatial operations of the R/V *Revelle* during the EXPORTS Northeast Pacific field deployment. (A) Broad categories of sampling events are marked by color, epoch boundaries are denoted by vertical dashed lines, and autonomous asset deployment periods are shown in gray. The epoch boundaries are given in UTC as Epoch 1, August 14 00:00 to August 23 09:00; Epoch 2, August 23 09:00 to August 31 09:00; and Epoch 3 August 31 09:00 to August 9 18:00. (B) Epochs and their spatial extent are delineated approximately by the autonomous assets deployed and recovered from the R/V *Revelle* (black dashed, purple, and blue lines) superimposed over the ship tracks (gray), with the first epoch in the south and the last epoch finishing in the most northeast of the EXPORTS experiment region. Locations of specific operations are color-coded to match those in (A). DOI: https://doi.org/10.1525/elementa.2020.00107.f9

thorium deficit, net community production, dissolved nutrients, oxygen, optical properties, and other constituents in the larger region surrounding the LF and Process Ship (**Table 2**). Vertical profiles were collected from the CTD-rosette system on both small (about 8-km spacing) and large (about 20-km spacing) scale grids for each epoch (**Figure 10**), with more intensive small-scale sampling in Epochs 1 and 3 and more intensive large-scale sampling in Epoch 2. Grids were centered on the location of the LF at the beginning of each epoch and were oriented so that the grid was perpendicular to the mean temperature and sea surface height fields. A complete suite of optical properties, including radiometric and inherent properties, were sampled at dawn and noon. Continuous underway samples for optical, biological, and selected chemical parameters were collected from an approximate 4-m depth with a flow-through system. Underway hyperspectral radiometry was collected during the day from the bow of the ship. Four pumping stations, with large volume pumps collecting particles at six to nine depths between 50 and

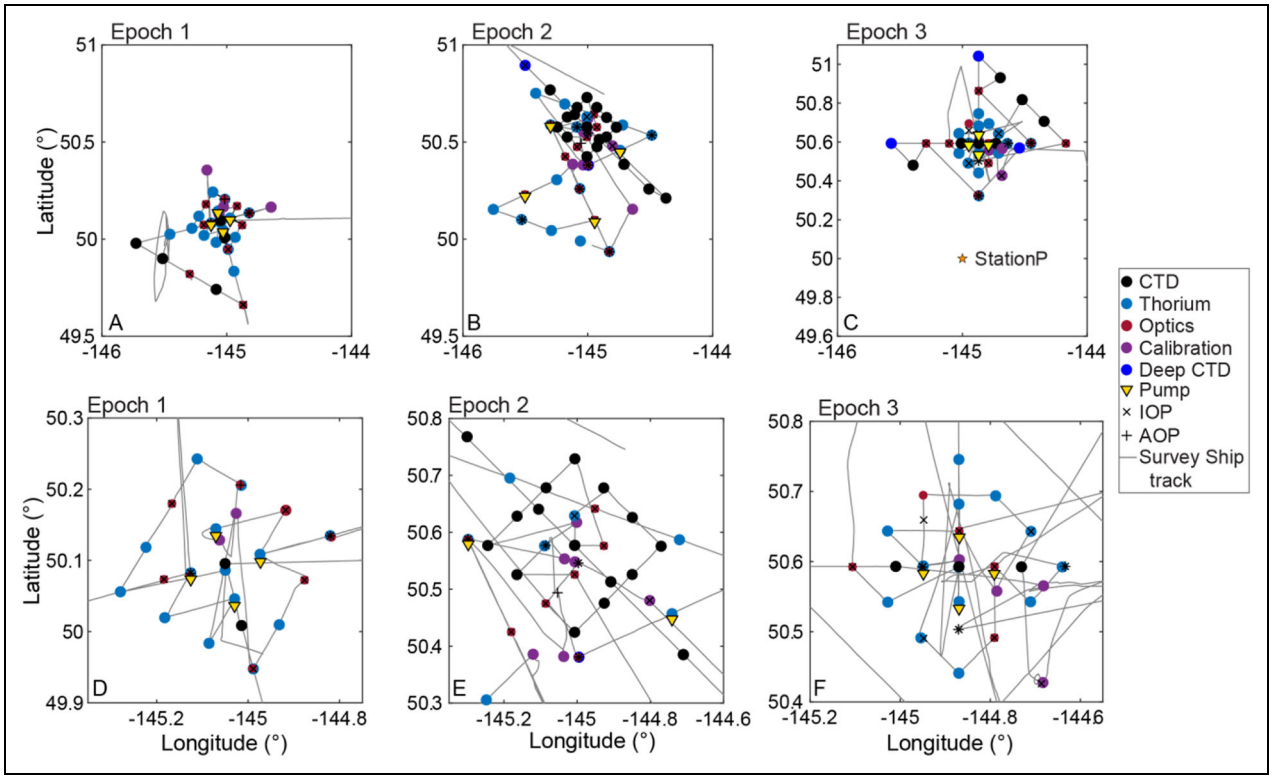

Figure 10. Sampling by the R/V *Ride* during the EXPORTS Northeast Pacific field deployment. Panels illustrate the sample locations and types of samples taken from the R/V *Ride* during the EXPORTS Northeast Pacific field deployment. Columns show panels for each sampling epoch, while top row illustrates on large spatial scales and bottom row shows an expanded view. Symbols indicate the main focus of sampling for each station: black circles, CTD profiles with sensors only (no bottles fired); blue circles, thorium collection; red circles, dawn (only inherent optical properties, IOP) and noon optics suite (radiometric and IOP); yellow-orange, intercalibration casts with the autonomous assets, Wirewalker, and R/V *Revelle*; and purple, deep CTD casts. Open triangles designate stations for large volume pumping and black x's and plus signs represent locations of radiometric and IOP casts, respectively (when not coincident with optics suite stations). DOI: https://doi.org/10.1525/elementa.2020.00107.f10

500 m, were carried out during each epoch, in coordination with the NBSTs.

A second task of the Survey Ship was to cross-calibrate sensors carried by the autonomous platforms and develop proxies for inferring biogeochemical parameters from sensor-based measurements. A total of 16 simultaneous ship CTD and autonomous asset profiles were collected (**Figure 10**): five for the LF, four for the Seaglider (SG), two for the BCG float, and three for the WW. These profiles were conducted to maximize spatial and temporal collocation of deliberate intercalibration casts by holding the target platform at the surface, moving the Survey Ship, which carried the designated reference sensors, into proximity (typically <300 m), and then simultaneously beginning profiles from both platforms. This approach facilitated alignment of all sensors against the reference units carried aboard the Survey Ship, allowing quantitative calculations that involve the entire array.

Sampling with autonomous platforms complemented the Process and Survey ship observations by resolving physical and biogeochemical variability at shorter temporal and spatial scales, and by expanding the sampling period to capture a broader range of physical and biological conditions (**Table 2**). A Seaglider (Eriksen et al., 2001), deployed on July 27 from the R/V *Ride* during the cruise, characterized mesoscale variability at the target site by occupying two repeats of a 25 by 25 km "bow tie" survey (**Figure 11**), at roughly 5-km horizontal resolution and 1-m vertical resolution, in the 2 weeks prior to the arrival of the EXPORTS ships. An instrumented Lagrangian float (D'Asaro, 2003), deployed from the Survey Ship on 14 August, defined a drifting reference frame used to target measurements through the three epochs and facilitate budget calculations just below the euphotic zone. The float was programmed to drift on an isopycnal near 100 m, with once-a-day surfacing. With the arrival of the ships and start of epoch-based sampling, the SG abandoned the "bowtie" survey to provide profiles at roughly 5-h resolution following the LF. A Wirewalker (Rainville and Pinkel, 2001), deployed near the LF at the start of each of the three epochs, profiled rapidly through the upper 500 m at intervals of 35–40 min.

Long-term sampling was conducted using two BGC profiling floats (Seabird Electronics Navis BGCi + pH). These were deployed on 15 August near Ocean Station P and on 17 August in proximity of the LF. During the EXPORTS field campaign BGC floats sampled in bursts, collecting three profiles, one from 2000-m depth and two

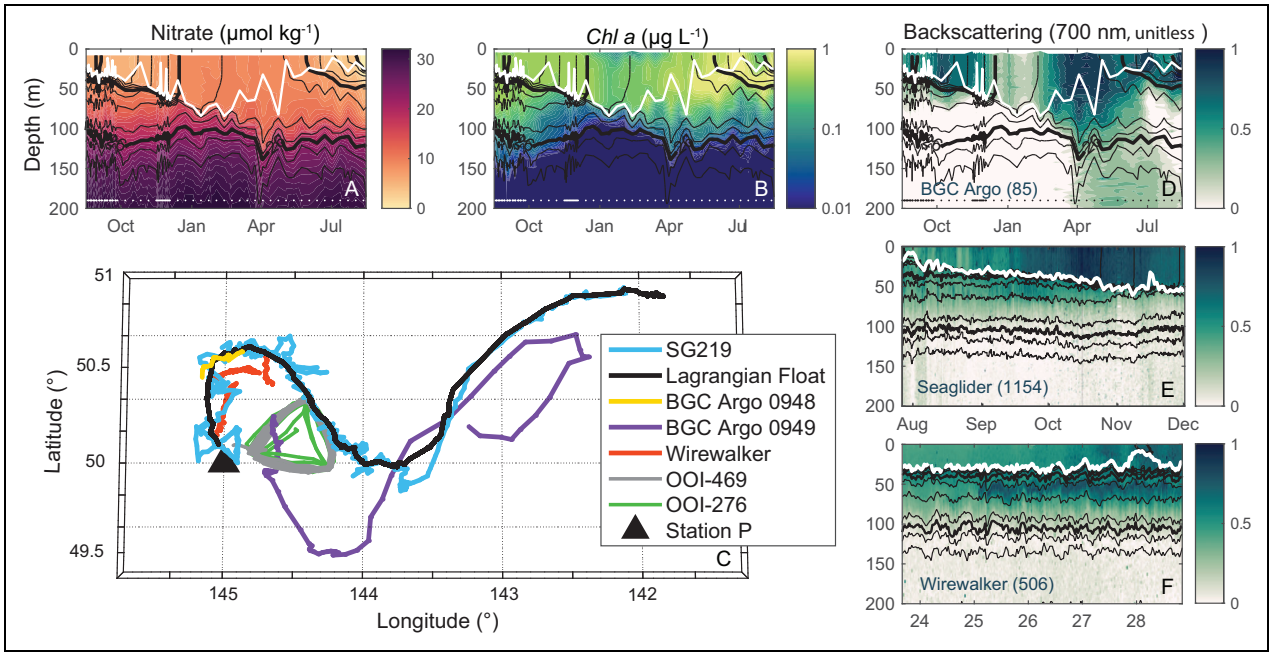

Figure 11. Autonomous platform operations during the EXPORTS Northeast Pacific field deployment. Time series measurements are shown for (A) nitrate and (B) *Chl a* concentrations from biogeochemical (BGC) float 0949 profiles (August 16, 2018, to August 15, 2019), along with (C) a map of the positions of autonomous assets operating in the region before, during, and after (up to August 15, 2019) the intensive portion of the EXPORTS field campaign. Also shown are time series profiles of particulate backscattering from (D) BGC float (BGC-0049; August 16, 2018 to August 15, 2019), (E) Seaglider (July 27, 2018 to December 1, 2018), and (F) Wirewalker (August 23, 2018 to August 31, 2018). These panels show preliminary backscattering data (unitless) that have been scaled to allow for qualitative comparison between platforms. The black contour lines in each plot are the potential density surfaces, and the white line is an estimate of the mixed layer depth. Values in parentheses represent the number of profiles contributing to the time series shown for each platform. This number is the same for all BGC (panels A–C). Dots at 190 m in the BGC float panels indicate profile frequency. DOI: https://doi.org/10.1525/elementa.2020.00107.f11

subsequent profiles from 500-m depth, over 24 h, with a 3-day interval between 24-h bursts. After the EXPORTS campaign, one of the BGC floats was recovered due to malfunction and the other BGC float reverted to the standard 10-day Argo profiling interval. The SG and LF sampled until recovery on December 1, 2018, while the BGC float (BGC-0049; Dory) was still operating as of the submission of this manuscript (March 2021). Additional measurements were provided by two Slocum gliders and moorings operating nearby as part of the OOI Station Papa Array. The BGC floats, LF, SG, and WW provide sampling at temporal resolutions spanning minutes to days and persistence across two annual cycles (**Figure 11**). The array of autonomous platforms, combined with ship-based observations, also allow characterizing mesoscale and submesoscale spatial variability.

Quantitative interpretation of the sensor-based measurements provided by autonomous platforms relies on careful calibration and intercalibration across the entire sensor array. This task was accomplished by performing bulk, pre-deployment laboratory calibration of all sensors (ship- and autonomous platform-based), deliberate in situ intercalibration (detailed above), and post-deployment laboratory calibration. Unplanned close encounters between platforms offered additional opportunities for intercalibration.

The Canadian Line P program partnered with EXPORTS by adding additional stations and measurements to their regular hydrographic sampling program following the EXPORTS cruise. The main objectives for this contribution were to: 1) provide an additional time point to the EXPORTS time series, 2) add measurements unique to the Canadian team, 3) intercalibrate nutrient and high-performance liquid chromatography (HPLC) methods used on the Line P program with those used on EXPORTS, and 4) perform a small spatial survey of mesoscale variability. Sampling was conducted September 20–22, 2018, 12 days after the completion of the main EXPORTS shipboard sampling (**Table 3**; **Figure 5**). In addition to sampling at Station P and the NOAA PMEL mooring as part of the regular time series, intensive sampling with multiple casts was conducted at EX-C, the location of the subsurface Lagrangian float (within a ship length for the LF calibration cast), and reduced sampling at an additional four satellite stations, one of which (EX-F1) was the location of BGC float "Dory" (BGC-0049). Sampling included regular hydrographic parameters, productivity rate measurements, ^{234}Th, large volume pumping, trace metals, organic

Table 3. Summary of measurements performed by Line P program in September 2018. DOI: https://doi.org/10.1525/elementa.2020.00107.t3

Measurement	Principal Investigator (Affiliation)	Station Locations[a]
CTD, salinity, O_2, NO_3, PO_4, H_4SiO_4, *Chl a*, phaeopigments	Robert (DFO)	EX-C, EX-F1, EX-W, EX-N, EX-E, Stn P
Net community production from O_2/Ar, O_2	Hamme (UVic)	EX-C, EX-F1, EX-W, EX-N, EX-E, Stn P
Export production from ^{234}Th	Buesseler (WHOI), Francois (UBC)	EX-C, EX-F1, EX-W, EX-N, EX-E
Large volume pumping	Francois (UBC)	EX-C
On deck incubations: primary production from ^{13}C, new production from ^{15}N-NO_3, recycled production from ^{15}N-NH_4, recycled production from ^{15}N-urea, SiO_2 production from ^{32}Si	Varela (UVic)	EX-C
NO_3, PO_4, H_4SiO_4, NH_4, urea, size-fractioned *Chl a* and biogenic silica	Varela (UVic), Hamme (UVic)	EX-C
On deck incubation: gross oxygen production from ^{18}O-H_2O	Hamme (UVic)	EX-C
Gross oxygen production from triple oxygen isotopes	Quay (UW)	EX-C
Trace metals	Cullen (UVic)	EX-C, EX-W, EX-N
TOC, DOC, CDOM, PIC, POC, gels	Johannessen (DFO), Hansell (RSMAS)	EX-C, EX-F1, EX-W, EX-N, EX-E
pH	Ianson (DFO)	EX-C, EX-F1, EX-W, EX-N, EX-E, Stn P
DIC, alkalinity	Ianson (DFO)	EX-C, EX-F1, Stn P
HPLC pigments	Pena (DFO)	EX-C, EX-W, EX-N, EX-E, Stn P
N_2O	Tortell (UBC)	EX-C, EX-F1, EX-W, EX-N, EX-E
DMS, DMSP	Arychuk (DFO)	EX-C, Stn P
Multi-omics	Carlson (UCSB), Marchetti (UNC)	EX-C

[a]Station locations: EX-C (Lagrangian float): 50.31°N 144.37°W, EX-F1 (BGC float): 49.96°N 144.70°W, EX-W: 50.38°N 144.64°W, EX-N: 50.61°N 144.06°W, EX-E: 50.18°N 144.14°W (see **Figure 6**).

carbon, carbon system parameters, pigments, dissolved gases, and multi-omics (**Table 3**).

The large collection of assets as well as the need to intercalibrate across these platforms required both real-time coordination for all platforms and a formal situational awareness capability to inform near-term planning and support adaptive sampling. The location for nearly all elements of the EXPORTS sampling array were tracked in real time and made available to the ship and AUV operators every 5 min. The complexity of the field logistics also required that multiple lines of communication were shared between ship- and shore-based team members. Situational awareness reports were created daily describing weather and ocean conditions as well as the operations performed and planned on the Process and Survey Ships, and the AUV array. The daily reporting allowed progress and status of all platforms to be monitored, facilitated democratic decision-making, increased coordination among measurement efforts and partnering research programs, and supported adaptive sampling and risk mitigation.

Parameters measured and data availability

The EXPORTS Implementation Plan (EXPORTS Science Definition Team, 2016) provided a table of essential and advantageous measurements needed to answer the EXPORTS science questions (Section 7.2 in EXPORTS Science Definition Team, 2016). These needs were used to estimate the cost of the different scenarios evaluated in the EXPORTS Implementation Plan. Once the EXPORTS science team was selected, parameter working groups were formed to organize the measurement suite and cruise planning. The five working groups were: (1) Stocks, Proxies, and Context; (2) Optics; (3) Particle Characterization; (4) Rates; and (5) Export Pathways. Their goals were to account for all measurements to be made, reconcile any duplication in effort across the science team, assemble sampling and measurement protocols for each measurement, and create a master table of parameters (**Table 4**). The parameter working group report (EXPORTS Science Team, 2020) provides short methodological descriptions for each parameter and the master table of parameters and data availability can be accessed at https://sites.google.com/view/oceanexports/home.

Table 4. Summary of the parameter working group objectives and measurements. DOI: https://doi.org/10.1525/elementa.2020.00107.t4

Working Group	Objectives	Type of Measurements/Instruments
Stocks, proxies and context	Document the stock, proxy, and context observations needed to interpret the other observations	Stocks are biogeochemical measurements in quantity per volume or mass seawater (e.g., dissolved organic carbon, dissolved oxygen). Proxies are synthesized observations created by mapping one variable onto another (e.g., particulate organic carbon derived from optical backscatter). Context observations include physical-sensor measurements from the EXPORTS assets (i.e., ships, autonomous vehicles, floats, moorings and remote sensing observations).
Optics	Provide high quality optical data that can be used to develop biogeochemical proxies and used to develop satellite algorithms using the EXPORTS observations	Apparent optical properties (e.g., radiance, irradiance, remote-sensing reflectance) and inherent optical properties (e.g., beam attenuation and absorption coefficients, volume scattering function) provide the links between EXPORTS observations and remote sensing algorithms. Measurements include those from ship underway system, ship-deployed profilers, above water radiometer, gliders, Lagrangian and BGC Argo floats and Wirewalker.
Particle characterization	Provide high quality measurements of the abundance, composition and size distribution of suspended particles (including live organisms) in the water column	Optical, chemical and imaging determination of the enumeration, sizing and classification of particles (e.g., plankton taxonomy and functional groups, biomass, biovolume, abundance, size distribution). Measurements were complemented with (1) metagenomics and DNA barcoding, (2) microscopic image analyses of particles, and (3) characterization of particles collected on polyacrylamide gels in sediment traps, zooplankton nets or in Marine Snow Catcher deployments. Instrumentation used includes, e.g., epifluorescence microscopy, flow cytometry, ImaginFlowCytoBot, ZooScan, Underwater Video Profiler, Coulter counter.
Rates	Provide high quality measurements of primary production, community, bacterial, secondary and grazing rates	Rates of primary productivity (GPP, NPP, NCP) are determined via the incorporation of isotopes (stable and radioactive) over 6- and 24-h incubations to measure uptake of dissolved inorganic carbon, nitrogen and silicon; the production of biogenic gases (e.g., oxygen) to estimate GPP, PP and NCP. Respiration metrics are determined for bacterial and community respiration by O_2 drawdown assays and DOC remineralization assays. Zooplankton respiration rates are assessed by O_2 drawdown, analysis of electron transport system enzyme activity, and converting community composition and biomass measurements to community respiration. Also included are bacterial production, secondary production and grazing, aggregation and sinking rates, and nutrient uptake rates.
Export	Understand the mechanisms controlling the magnitude and attenuation of the primary export pathway fluxes	Sinking particle rates are estimated using arrays of sediment traps, radionuclide mass balances, Marine Snow Catcher deployments and the numerical modeling of suspended and sinking particle organic carbon distributions. Assessments of the zooplankton-mediated migrant fluxes used day-night MOCNESS zooplankton biomass distributions along with assessments of zooplankton respiration and dissolved organic carbon and fecal production rates. Flux composition is assessed using high magnification microscope images of polyacrylamide gel collectors on sediment traps, genetic sequencing, image analyses on collected and in situ samples and contributions to bulk traps of amino acids. Processes regulating the vertical attenuation of sinking particle fluxes were determined using RESPIRE traps, Underwater Vision Profile images and the modeling of aggregate dynamics and coagulation.

Data generated during EXPORTS follow the NASA Earth Science Data and Information Policy (http://science.nasa.gov/earth-science/earth-science-data/data-information-policy/), which requires data to be available from a designated long-term public data repository within a year of collection. NASA-funded primary data products are archived at SeaWiFS Bio-optical Archive and Storage System (SeaBASS). All EXPORTS data are being archived under one digital object identifier (DOI: http://dx.doi.org/10.5067/SeaBASS/EXPORTS/DATA001) that further expands into the individual data subsets. NSF-funded primary data products are archived and distributed by the Biological and Chemical Oceanographic-Data Management Office (BCO-DMO). The BCO-DMO EXPORTS data-products webpage provides access to all the NSF-funded EXPORTS projects and links to the individual data set (https://www.bco-dmo.org/program/757397), where each individual data set has a unique doi. Data sets that cannot be handled

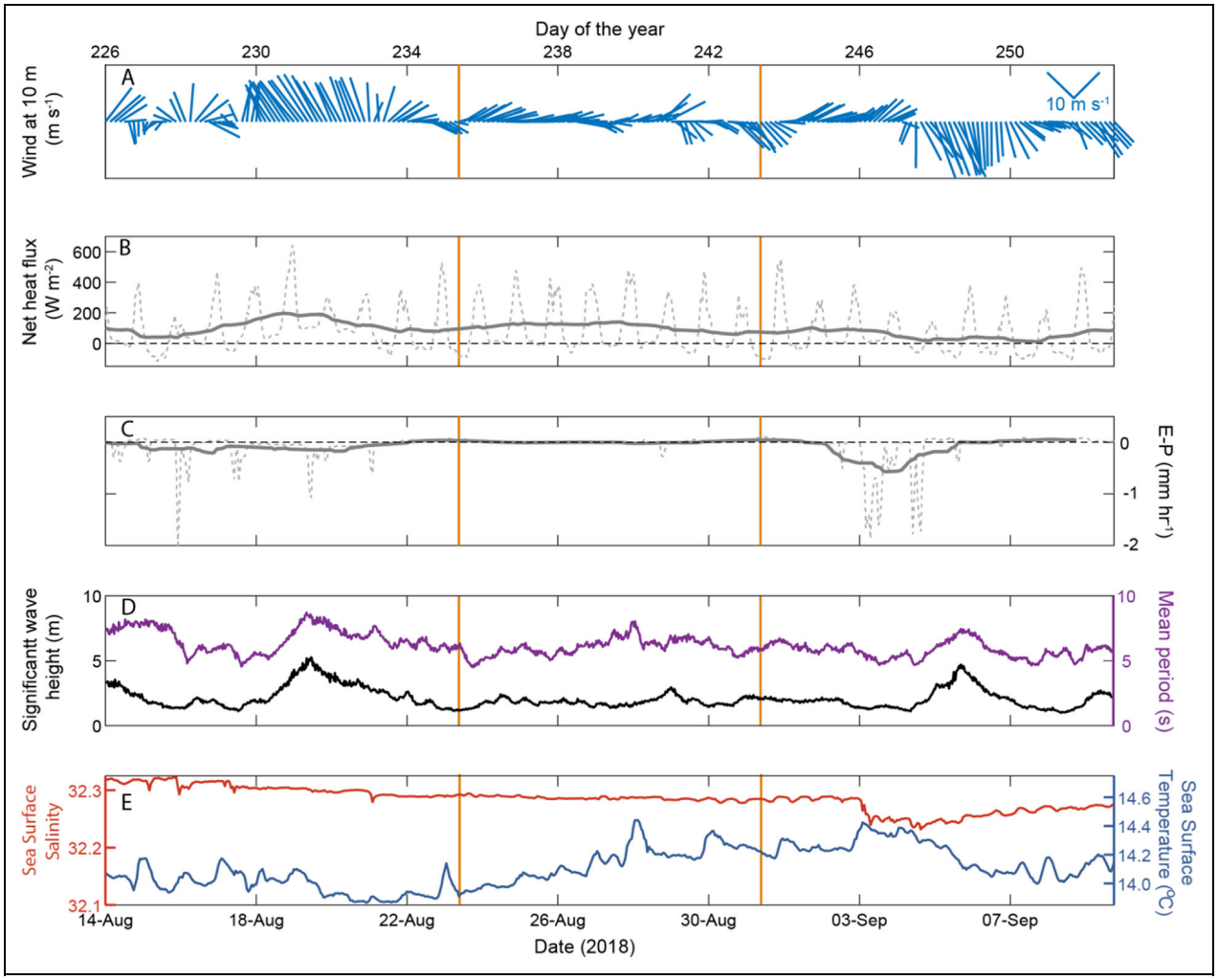

Figure 12. Air–sea fluxes from the NOAA PMEL air-sea interactions buoy. From the top are shown (A) daily wind speed and direction, (B) net air–sea heat flux, (C) evaporation-precipitation (E-P), (D) significant wave height and period, and (E) sea surface temperature and salinity measured from the NOAA PMEL air-sea interaction mooring (www.pmel.noaa.gov/ocs/data/disdel) and the UW-APL waverider buoy (www.apl.washington.edu/projects/station_papa/summary.html) during the period of the three ship-sampling epochs (from 14 August to September 9, 2018). DOI: https://doi.org/10.1525/elementa.2020.00107.f12

within the main NASA and NSF databases, such as genetic, microimaging, and taxonomic data, will be deposited in appropriate community data repositories. Links to all data sets will be provided through the master table of parameters (https://sites.google.com/view/oceanexports/home) and the Project website (https://oceanexports.org/).

Oceanographic setting during the 2018 EXPORTS Northeast Pacific deployment

Presented in this section are fundamental observations from the EXPORTS NE Pacific Field Campaign to help contextualize information provided by other manuscripts in this special collection. Time series of air–sea momentum, heat and freshwater fluxes, as well as wave and surface ocean physical properties, from the NOAA PMEL and UW-APL moorings are shown in **Figure 12**. During the three epochs, net heat fluxes were generally into the ocean leading to warming of the mixed layer; however, during Epoch 3 heat inputs were reduced. The three epochs can be distinguished from each other by their weather events (or lack thereof). Epoch 1 had a southerly storm that brought winds in excess of 12 m s^{-1} and significant wave heights approaching 5 m during the latter half of the epoch. This storm hampered the collection of field samples from both ships. Epoch 2 was distinguished by relatively calm conditions, and mixed layer heating was observed as sea surface temperature (SST) at the NOAA PMEL mooring increased by roughly 0.3 °C over the 8 days of the epoch. Epoch 3 had a northerly storm of similar magnitude to that in Epoch 1 and a large precipitation event on 4 September (year day 247). Again, this weather slowed the collection of samples, particularly for the R/V *Sally Ride*. A decline in sea surface salinity (by approximately 0.05) was seen at the NOAA PMEL mooring site during Epoch 3, consistent with these freshwater inputs (**Figure 12**).

The large-scale features for both sea surface height (SSH) and SST show lower SSH and cooler SST in the northwest portion of the domain with both parameters

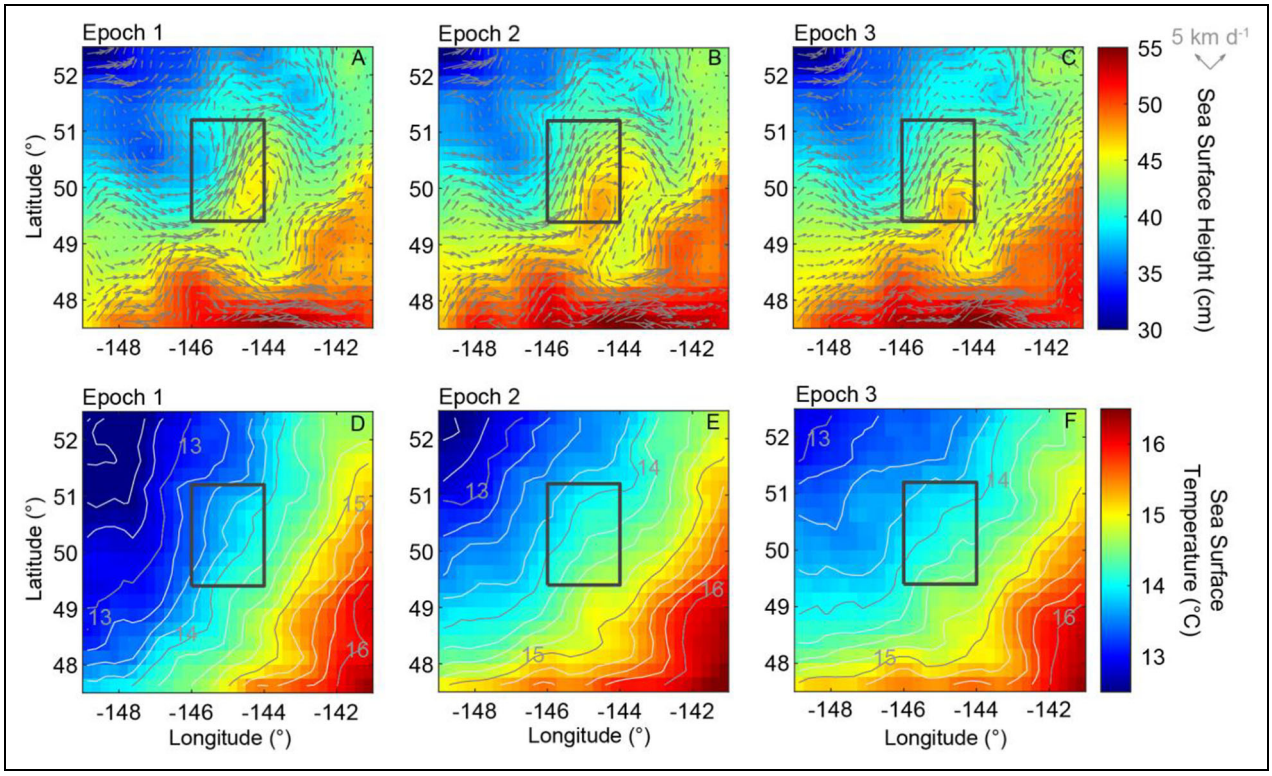

Figure 13. Spatial maps of sea surface height and sea surface temperature during the EXPORTS sampling epochs. Spatial maps of (upper) absolute sea surface height from merged daily satellite altimetry and (lower) sea surface temperature (SST) for the three EXPORTS sampling epochs (left to right). Daily, near-real time, and gridded (0.25° resolution) absolute sea surface height were used to create these distributions (resources.marine.copernicus.eu/?option=com_csw&view=details&product_id=SEALEVEL_GLO_PHY_L4_NRT_OBSERVATIONS_008_046). Optimally interpolated passive microwave (cloud penetrating) SST daily products (25-km resolution) were used as the SST products (www.remss.com/measurements/sea-surface-temperature/oisst-description). The black boxes indicate the sampling regions for the EXPORTS field deployment shown in **Figure 6B**. DOI: https://doi.org/10.1525/elementa.2020.00107.f13

increasing to the southeast (**Figure 13**). The EXPORTS assets were deployed to the northwest of an anticyclonic mesoscale feature creating a north-northeast current that was reflected in the drift of the Lagrangian float (**Figure 11C**). The SSH and SST patterns were similar for each epoch with a hint of an intensification of the mesoscale feature in time and an increase in SST during Epoch 2 and a cooling in Epoch 3.

Minimal satellite ocean color imagery was available during the intensive operations period due to the persistent cloud cover (**Figure 14**). For August–September multiple satellite composites had better coverage, with most of the clear-sky views occurring in late September. A weak increase in satellite *Chl a* concentrations (about 0.1 mg m^{-3}) appears associated with the location of the anti-cyclonic feature noted in the SSH fields, but even this feature is difficult to distinguish.

Time series of upper layer temperature and salinity from the R/V *Revelle*'s underway flow-through system (**Figure 15A**) reflects many of the same general patterns observed at the NOAA PMEL mooring (**Figure 12**); that is, approximately stable SST and sea surface salinity relationships are found in Epoch 1, heating during Epoch 2, and change in surface water masses during Epoch 3. In particular, the influence of rain inputs is clear in this record during Epoch 3 (5 and 6 September).

Acoustic Doppler current profiler observations of mixed layer currents from the R/V *Revelle* show small sub-inertial currents, typically 2–3 km d^{-1} (1 km d^{-1} = 1.157 cm s^{-1}; **Figure 15B** and **C**). These low values support the notion that Station P has unusually low mesoscale kinetic energy compared with most other open ocean sites. During Epoch 1 and through the first part of Epoch 2, sub-inertial surface currents were comparatively large (about 4 km d^{-1}) and flow was consistently to the north (**Figure 15B**). After that, sub-inertial currents were sluggish ($\leq$2 km d^{-1}) until the very end of Epoch 3. Mixed layer currents were dominated by supra-inertial frequency motions, where root mean square of the 15-min averaged current speeds (approximately 14.5 km d^{-1}) are more than five times greater than the root mean square of the two-day averaged currents (**Figure 15C**).

Estimates of MLD were determined using CTD/rosette data from both ships as the first depth where the potential density exceeds the density at 50 m by 0.1 kg m^{-3} (**Figure 15D**). Values of MLD varied from 20 to 35 m with a mean depth of 31 $\pm$ 4 m (n = 227). Changes in time show a temporal pattern roughly similar to SST, where higher

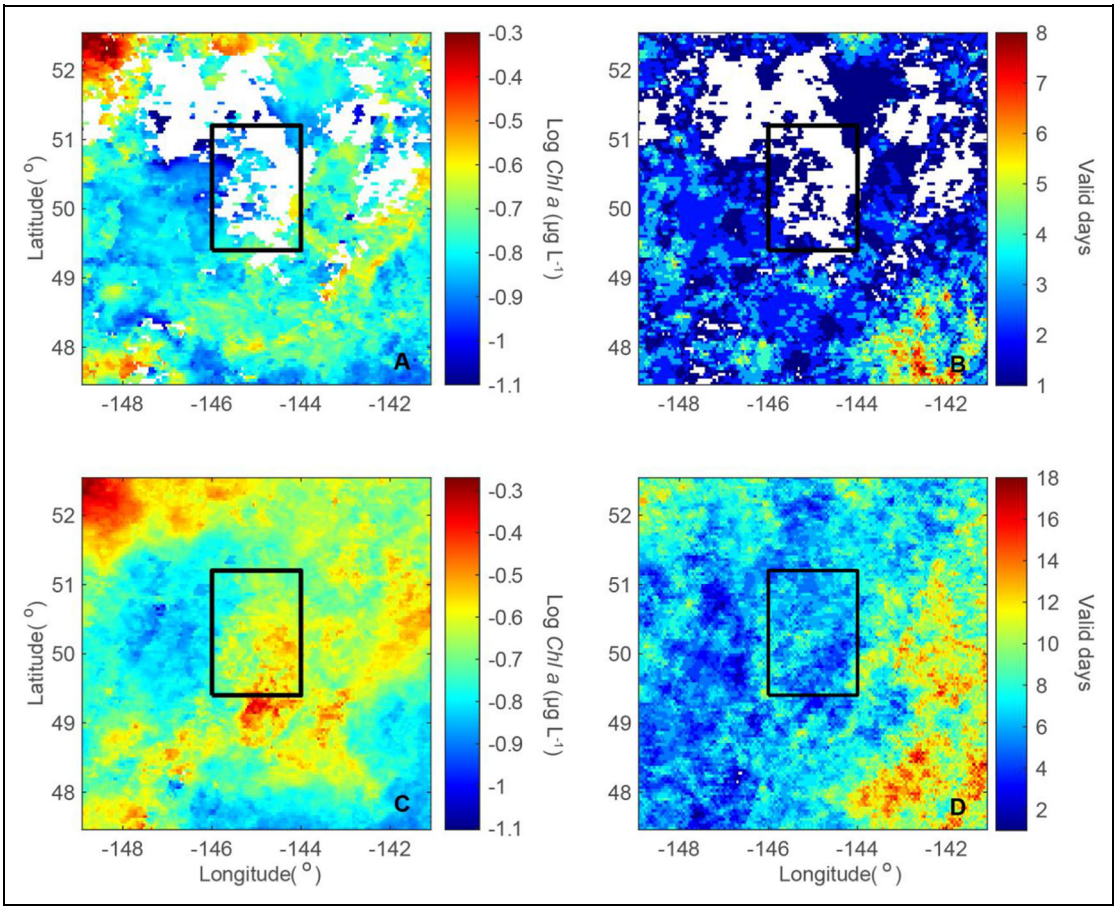

Figure 14. Composite satellite ocean color *Chl a* concentration imagery during the EXPORTS field deployment. Composite $\log_{10}$-transformed *Chl a* concentrations for the ship sampling period at Station P (14 August to September 9, 2018) are shown in the upper and lower left panels (A, C) for the respective months of August and September 2018. Corresponding images for the number of valid days for each composite are shown in the two panels on the right (B, D). The composite *Chl a* imagery was created from daily merged observations (1/24 at approximate 4-km resolution) from all available MODIS and VIIRS images (https://oceandata.sci.gsfc.nasa.gov/opendap/Merged_ATV/L3SMI/2018). The black boxes indicate the sampling regions for the EXPORTS field deployment shown in **Figure 6B**. DOI: https://doi.org/10.1525/elementa.2020.00107.f14

SSTs appear to correspond to shallower MLD determinations.

Daily integrated rates of incident PAR fluxes from the R/V *Revelle* varied nearly four-fold over the experiment (**Figure 15E**). Integrated daily incident PAR values were derived from the underway PAR data, collected every 15s on each ship, that have been cross-calibrated to the Compact-Optical Profiling System (C-OPS, Biospherical Instruments, Inc) deck sensor data before integration from local sunrise to sunset. Values of incident PAR varied 5-fold from 10 to nearly 40 moles photons m^{-2} d^{-1} with the highest incident PAR fluxes found in the second epoch and the lowest in the third.

Bio-optical estimates of phytoplankton carbon (C_{phyto}) and *Chl a* concentrations were made using the R/V *Revelle's* underway system (**Figure 15F**). Particulate backscattering coefficient observations at 470 nm were used to estimate C_{phyto} concentrations following Graff et al. (2015). Estimates of *Chl* a concentrations were made using particulate absorption line height at 676-nm determinations (Boss et al., 2013) and calibrated with coincident HPLC determinations of total *Chl a* concentrations collected during the campaign (*Chl* a = 138.14 × line_height$^{1.11}$; r^2 = 0.67; n = 43). In general, near-surface *Chl a* concentrations were low with mean concentrations of 0.21 µg L^{-1} (**Figure 15F**), considerably less than typical August values for Station P (**Figure 7F**). Variability is observed, as *Chl a* values ranged from approximately 0.10 to 0.35 µg L^{-1}, although changes in epoch mean *Chl a* values were small (approximately 0.01 µg L^{-1}). The highest values are found near the middle of the first epoch (around day 232 or August 22), while the lowest values are found in the period between Epochs 1 and 2. Changes in the C_{phyto} concentrations generally follow the behavior of *Chl a*, but their amplitude of changes are comparatively muted. Large short-duration departures in the underway *Chl a* concentrations are also observed in the data set at times (for example, see 23 August; **Figure 15**). These anomalies often coincide with "poop runs" for the R/V *Revelle* as the ship leaves its Lagrangian sampling frame.

Euphotic zone depths were estimated using depths of 1% incident PAR (Z_{eu}; **Figure 15G**). Values of Z_{eu} were

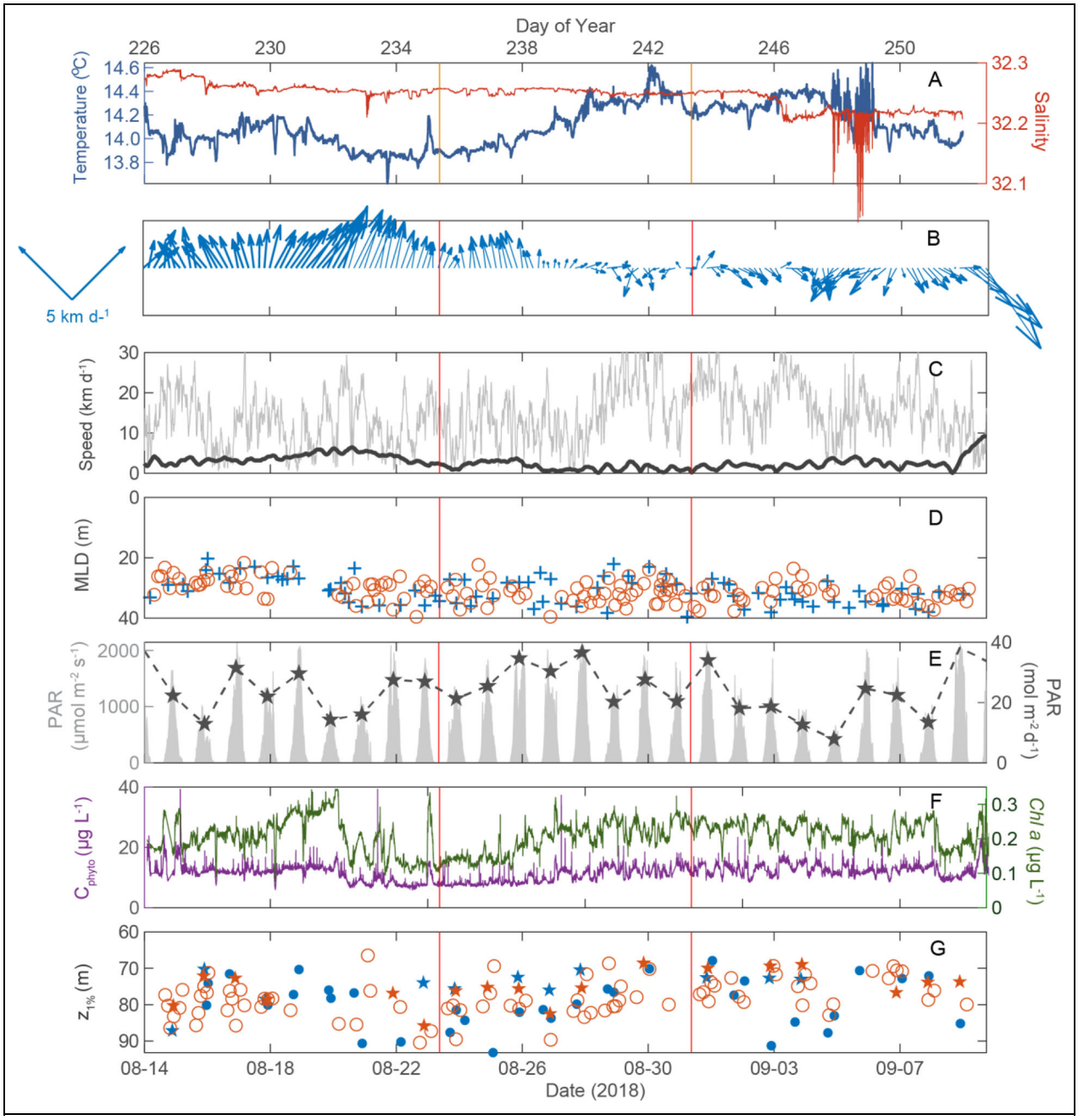

Figure 15. Oceanographic time series from the R/V *Revelle* and the R/V *Ride*. (A) Time series of temperature and salinity from the R/V *Revelle* underway sampling system (approximate 5-m depth intake). (B) Mixed layer currents (averaged between 20 and 35 m) from the R/V *Revelle* 150 kHz broadband ADCP system. The blue arrows show the low-passed (2-day filtered) mixed layer current magnitude and direction. (C) Root mean square (RMS) current speed from the R/V *Revelle* ADCP system. The gray line is the RMS of the 15-min averaged current speed, while the blue line is the RMS of the 2-day averaged currents. (D) mixed layer depth (MLD) estimates from the CTD profiles from the R/V *Revelle* (blue) and the R/V *Ride* (burnt orange). (E) Incident PAR flux (gray, left axis) and daily integrated PAR fluxes (blue, right axis). (F) Bio-optical estimates of phytoplankton carbon (black, left axis) and *Chl a* (green, right axis) concentrations from the R/V *Revelle*'s underway optics system. (G) Euphotic zone depths are estimated as the depth of the 1% PAR surface. Estimates from the R/V *Revelle* (blue) and the R/V *Ride* (burnt orange) are shown as well as values from the CTD-mounted PAR sensors (circles) and C-OPS spectroradiometry casts (stars). DOI: https://doi.org/10.1525/elementa.2020.00107.f15

determined from both ships using both PAR sensors mounted on the CTD/rosettes and hand-deployed spectroradiometer casts using C-OPS. These data were available from each ship, although C-OPS profiles were not conducted as often due to adverse weather conditions. Values of the vertical attenuation of PAR were calculated via robust linear regression over the depth range of 10–80 m and converted into estimates of the depth of the 1%

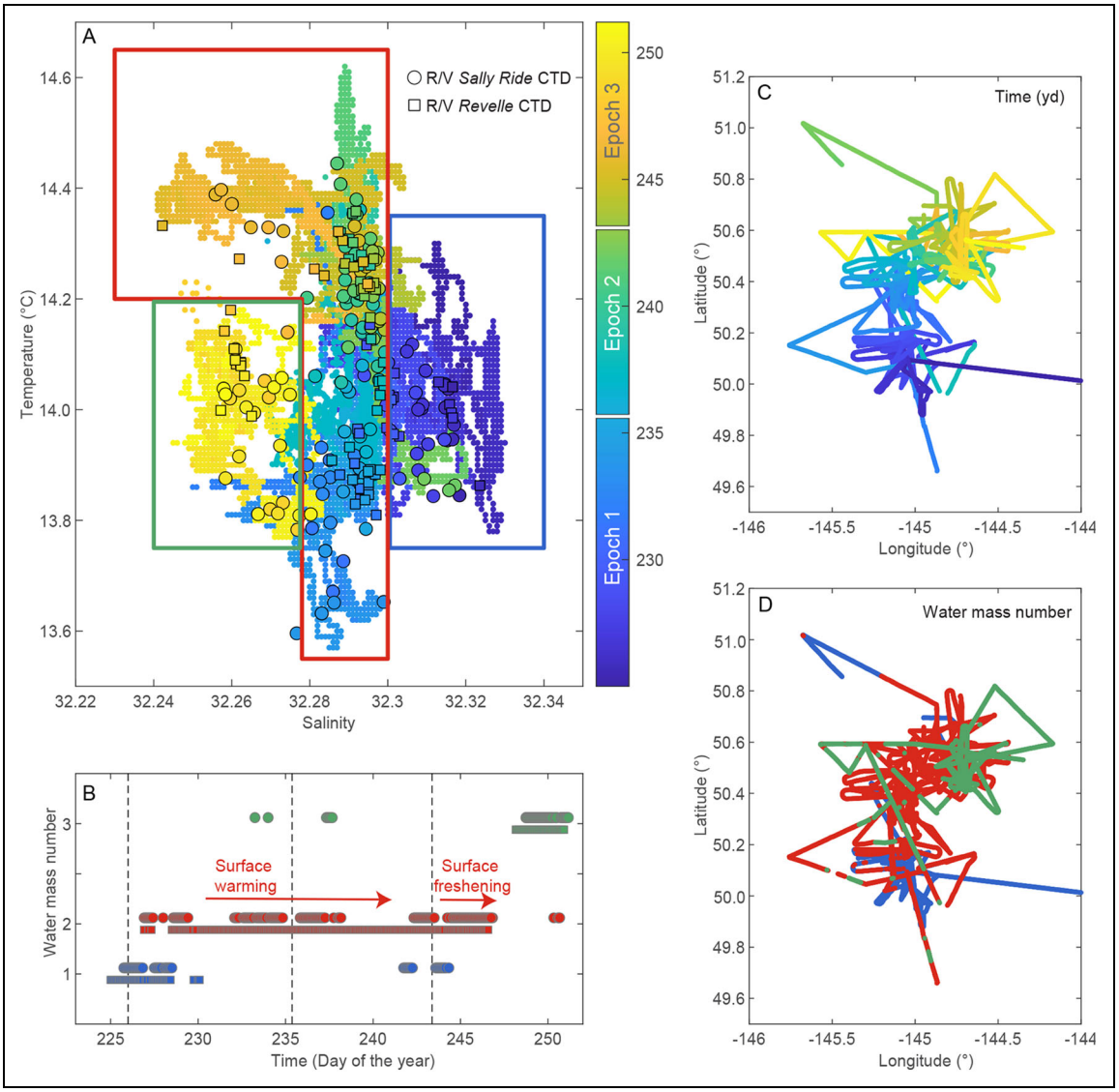

Figure 16. Variations in surface mixed layer water masses. (A) Distribution of temperature (°C) and salinity from underway measurements (both ships, dots) as well as R/V *Ride* (circles) and R/V *Revelle* (squares) CTD casts. For all symbols, color indicates the time of the measurement (year day). Three water masses, outlined by blue, red, and green curves, delineate separate water mass properties (see text for details). (B) Time series of the three surfaces water masses encountered by the R/V *Ride* (circles) and R/V *Revelle* (squares). The water mass identification is discretized in 0.2-day bins. Maps of the R/V *Ride* and *Revelle* positions colored by (C) time (year day) and (D) water mass index are shown in the right-hand panels. DOI: https://doi.org/10.1525/elementa.2020.00107.f16

incident PAR isolume (also assuming a 4% loss at the air/water interface). Vertical attenuation coefficients for PAR were averaged if multiple estimates were available for a particular day. Values of Z_{eu} ranged from 70 to 90 m with a good deal of variability with mean 1% PAR depth of 78 ± 6 m (n = 149; **Figure 15G**). Determinations of euphotic zone depth do not show a coherent pattern of change over time.

The variation of temperature (T) and salinity (S) properties in the surface mixed layer, as measured from both the ship-based CTD casts and the ships' underway measurements, was small, spanning roughly 1 °C (13.5 < T < 14.6 °C) and 1 (32.24 < S < 32.34) (**Figure 16A**). The temporal evolution of the measured surface properties in both space and time began with relatively salty surface properties (S = 32.32, T = 14 °C) that freshen and cool during most of Epoch 1. As discussed in detail below, the transition to cooler water was sampled during a period of net surface warming, suggesting that these cooler waters had a distinct origin. From the end of Epoch 1 and throughout Epoch 2, surface salinity remained largely constant (32.29), but surface temperature increased by roughly 1 °C between year day 232 and 241 (22 and 31 August). This rate of warming agrees well with the predicted surface warming based on surface flux data from the NOAA PMEL mooring (**Figure 17**). Around year day 244 (1 September) a distinct surface freshening was observed, bringing the salinity to values as low as 32.34, while temperature remained constant around 14.4 °C. The magnitude and timing of this freshening signal is

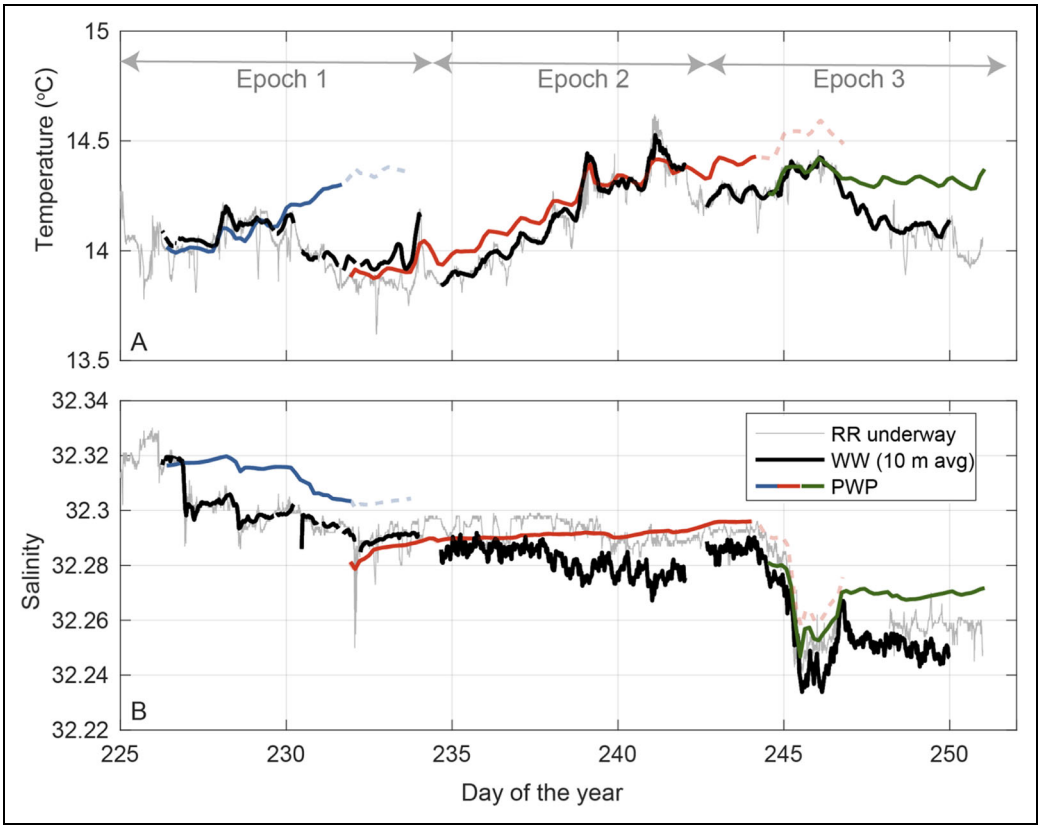

Figure 17. Time series of measured and model predicted temperature and salinity averaged over upper 10 m. Time series of (A) temperature and (B) salinity averaged over the upper 10 m from the PWP model (colored lines; see text for details), the Wirewalker (black lines) and the R/V *Revelle* underway system (gray lines). The PWP model was initialized at the start of each of the three water property groups. Dashed lines show the model predictions for a few days after each of these transitions, highlighting the departures between the 1D model (meteorological forcing only) and the observations (a combination of lateral advection and meteorological forcing). DOI: https://doi.org/10.1525/elementa.2020.00107.f17

consistent with a period of net precipitation. During the latter half of Epoch 3, SST dropped abruptly by about 0.3 °C, a change that did not coincide with a surface cooling. This feature represents the strongest surface front observed over the course of the experiment.

Based on these changes and an analysis of the surface flux data, we can identify three distinct groups of water properties in the mixed layer during the experiment (**Figure 16A**, **B**, and D). Groups 1 and 3 (blue and green, respectively, in **Figure 16**) are salty and fresh endmembers that were occupied at the beginning and end of the field program, respectively. The majority of the experiment, roughly year day 228–237 (August 16–25), sampled surface water in Group 2 (red in **Figure 16**) and covered the entire range of temperatures and a large fraction of the salinity values measured. However, near-surface water property changes during this period were well predicted by fluxes of surface heat, freshwater and momentum, suggesting that measurements made in the Group 2 period were largely in a Lagrangian framework following a fixed patch of surface water. The positions of the two ships with respect to time (year day) and to surface water type are shown in **Figure 16C** and **D**.

Isolating the advective changes from meteorological forcing (warming, freshening) in the mixed layer was accomplished by comparison with a one-dimensional Price-Weller-Pinkel model (PWP; Price et al., 1986). The PWP model uses the air–sea heat fluxes and wind stress to predict time- and depth-resolved variations in upper ocean S and T. The model was initialized with a CTD profile collected by the R/V *Revelle* at the beginning of each of the three water property groups defined above. Modeled T and S (colored lines, as per group, in **Figure 17**) was compared with T and S from the WW (black lines in **Figure 17**), both averaged over the upper 10 m, and with underway measurements from the RV *Revelle* (gray lines in **Figure 17**). Overall, the PWP model reproduced diel variations and the trend in surface warming, particularly that observed during Group 2. The model also successfully predicted the sharp freshening event that occurred on year day 245 (2 September during Epoch 3) after some prolonged precipitation.

Mean profiles of CTD sensor observations are shown in **Figure 18A–D** for T, S, potential density (σ_θ), and dissolved oxygen (O_2). The temperature profile (**Figure 18A**) shows a mixed layer of roughly 30 m and a strong seasonal thermocline, as was seen in the August Line P climatology for this site (**Figure 7A**). At this scale, few differences are apparent among the three epochs beyond Epoch 1 being slightly cooler than the other two from

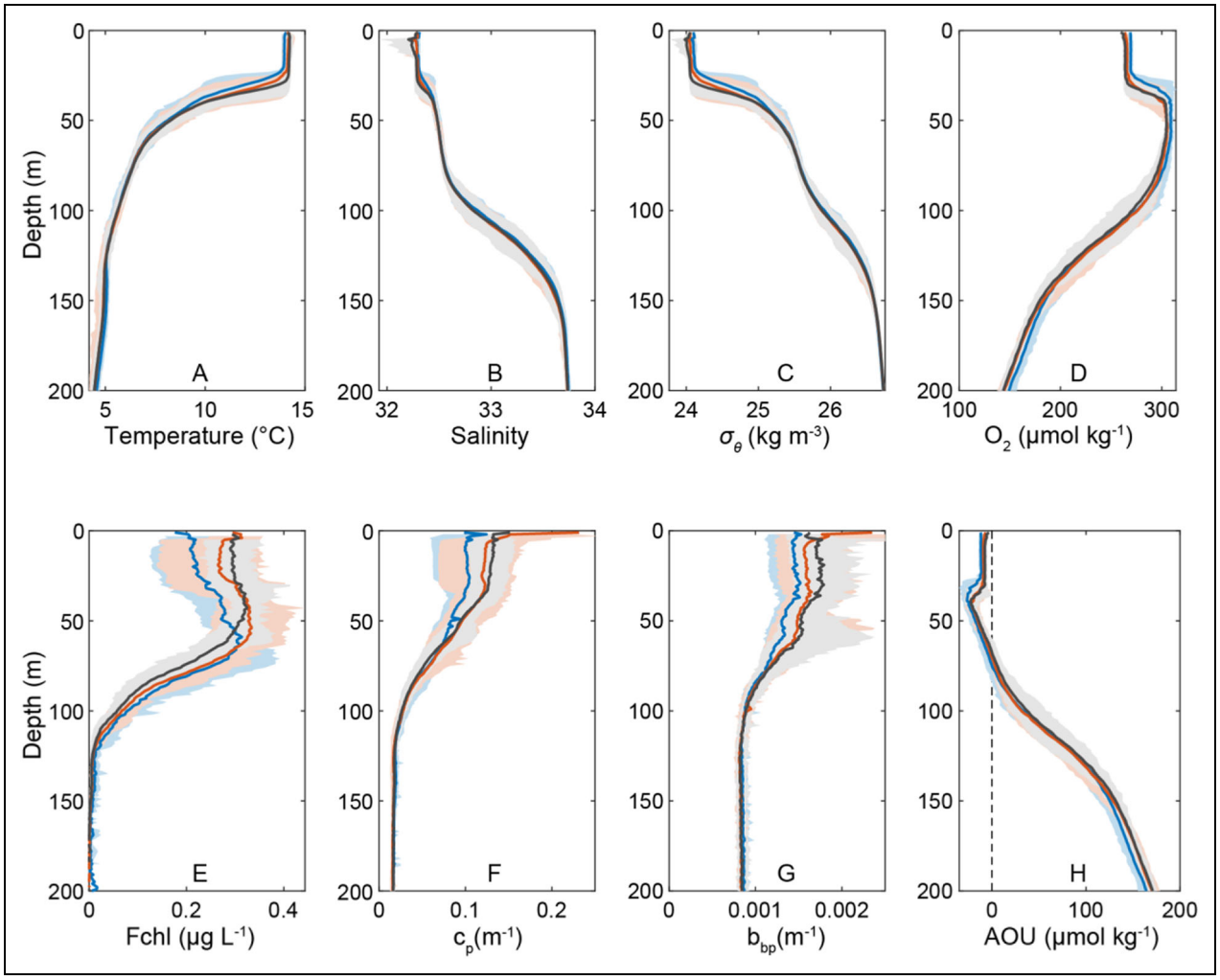

Figure 18. Sensor CTD data profiles from both ships. (A) Temperature, (B) salinity, (C) potential density (σ_θ), (D) dissolved oxygen (O_2), (E) chlorophyll fluorescence (Fchl, night time profiles only), (F) particulate beam attenuation coefficient at 700 nm (c_p), (G) particulate backscatter at 700 nm (b_{bp}), and (H) apparent oxygen utilization (AOU) for the three epochs (blue, orange, and black correspond to Epochs 1, 2, and 3, respectively). Envelopes are 95% confidence intervals for the mean estimates at each depth bin. Data from the R/V *Ride* are combined with data from the R/V *Revelle* when both ships were within 25 km of each other. DOI: https://doi.org/10.1525/elementa.2020.00107.f18

the surface to a depth of about 70 m. The salinity distribution shows a stabilizing profile throughout the upper 200 m of the water column and strong halocline from 100 to 140 m, which forms the permanent pycnocline. The potential density distribution (**Figure 18C**) shows the classic two pycnoclines for this site and a sharp MLD with few inversions. Dissolved oxygen concentrations are elevated in the mixed layer and in the layer directly beneath it (to about 100 m) and decrease rapidly beneath that depth.

The particulate beam attenuation coefficient at 700 nm (c_p) and the particulate backscattering coefficient at 700 nm (b_{bp}; **Figure 18F** and **G**) both account for the particle load within the water column, with values of c_p representative of larger particles compared to b_{bp} (e.g., Stramski and Kiefer, 1991; Zhang et al., 2020). Values of both c_p and b_{bp} are elevated in the upper 40 m and decrease to minimal values beneath that depth. The fractional reduction with depth for c_p is much greater than for b_{bp}, suggesting that a background of very small particles supported the b_{bp} signal (Zhang et al., 2020) or that the contributions of organic-dominant particles vs. mineral-dominant particles changed with depth (Cetinić et al., 2012). Mixed layer particle loads also tended to increase through the experiment. Values of AOU (**Figure 18H**) show supersaturation of dissolved oxygen concentrations in the upper 75 m of the water column, illustrating net autotrophy in the upper layers, particularly just beneath the mixed layer. Strongly negative AOU values are found at depth, illustrating the consumption of oxygen by respiration.

Nutrient profiles (**Figure 19B** and **C**) from water sampling conducted on the R/V *Revelle* show elevated concentrations (approximately 8 and 15 µmol kg^{-1} for NO_3 and SiO_4, respectively) in the upper 40 m increasing with depth (roughly 20 and 25 µmol kg^{-1} for NO_3 and SiO_4

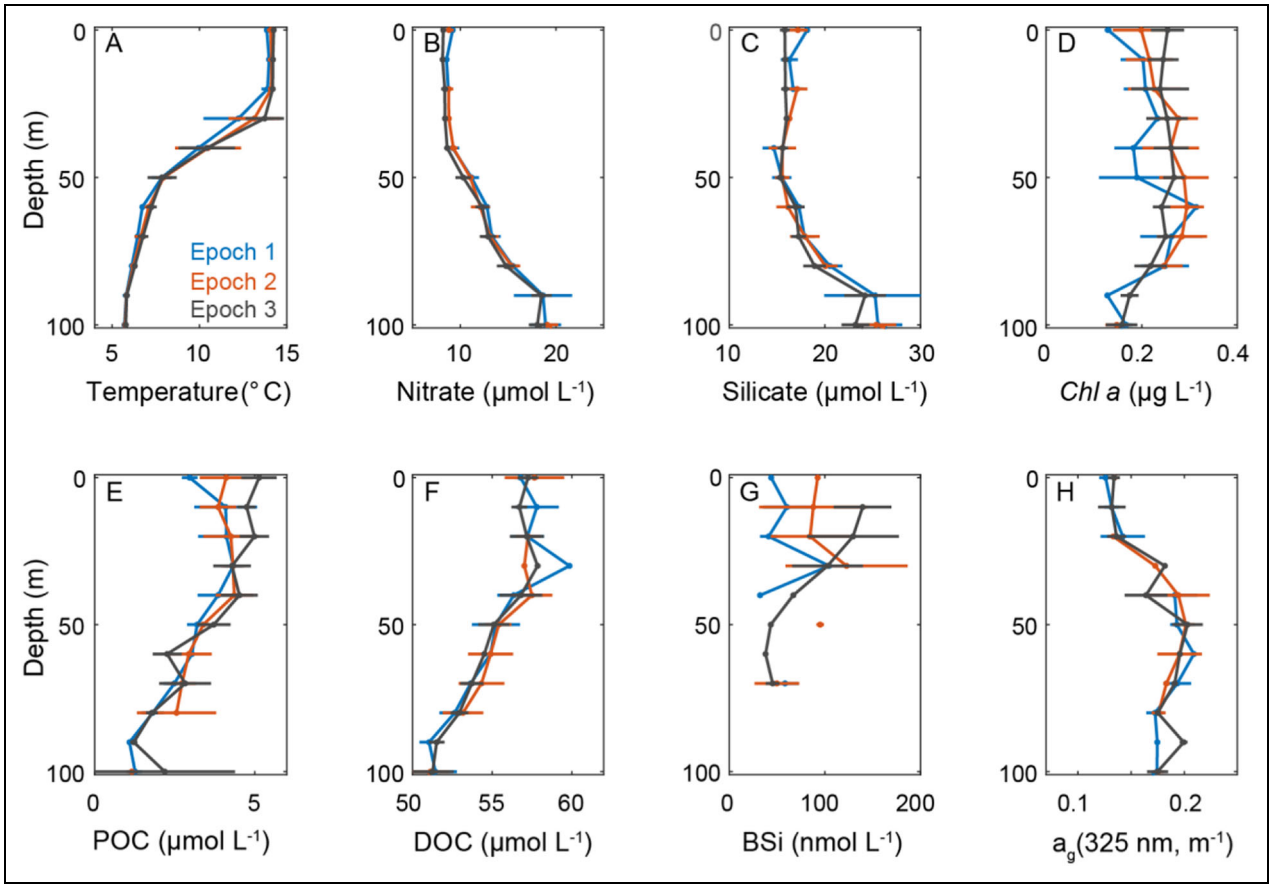

Figure 19. Vertical mean profile data for bottle samples, by epoch, for the R/V *Revelle*. Shown are the means with standard deviation (error bars) for (A) temperature (at bottle trip), (B) dissolved nitrate, (C) dissolved silicate, (D) *Chl a* by HPLC, (E) particulate organic carbon (POC), (F) dissolved organic carbon (DOC), (G) particulate biogenic silica (BSi) from the TMC rosette, and (H) absorption coefficient (a_g) of chromophoric dissolved organic matter at 325 nm. For each panel, blue is Epoch 1, orange is Epoch 2, and black is Epoch 3. DOI: https://doi.org/10.1525/elementa.2020.00107.f19

at 100 m, respectively). No apparent change is seen in nutrient concentrations among the epochs.

Profiles of *Chl a* concentration were determined from night-time fluorometer casts calibrated against total *Chl a* by HPLC (**Figure 18E**) or from discrete measurements (**Figure 19D**). Mixed layer values for the three epochs are roughly 0.2–0.3 μg L^{-1} with the lowest mixed layer *Chl a* concentration occurring in Epoch 1, consistent with the underway bio-optical proxies from the R/V *Revelle* (**Figure 15E**). A subsurface *Chl a* maximum is found at about 70 m, and *Chl a* values decrease beneath that to background levels at about 120 m. Changes in mixed layer biogenic silica concentrations largely mirror the changes in *Chl a* concentrations (**Figure 19G**).

Both POC and dissolved organic carbon (DOC) were elevated in the mixed layer and decreased below a depth of about 40 m (**Figures 19E** and **F**). Values of DOC in the mixed layer are more than four times the POC values. The reduction with depth in DOC is roughly twice as much as the reduction in POC concentrations (roughly 5 vs. 2.5 μmol L^{-1} for DOC and POC, respectively). DOC concentrations show little change over time, although mixed layer POC concentrations increased slightly in Epoch 3 (similar to *Chl a*). Values of the absorption coefficient for chromophoric dissolved organic matter (CDOM) at 325 nm (**Figure 19H**) increase from approximately 0.13 m^{-1} in the surface layer to 0.2 m^{-1} at 40 and 60 m. These CDOM values approach the highest seen in the global open ocean (Nelson and Siegel, 2013). Also apparent is the lack of correspondence between the mean vertical profiles for CDOM and DOC, illustrating that CDOM is a poor proxy for DOC concentrations.

Though not all collocated, autonomous platforms provided a longer-term perspective on the evolution of the physical and biogeochemical properties after the ships departed. Because the Seaglider closely followed the Lagrangian float (**Figure 11C**), changes in Seaglider-observed bio-optical properties (**Figure 11E**) generally reflect growth and losses in phytoplankton rather than spatial heterogeneity. By mid-October 2018, a phytoplankton bloom had developed, largely in the surface mixed layer. Coinciding with this event, spikes in b_{bp} increased and persisted throughout November and December. The mixed layer reached a maximum of around 100 m in early 2019 (**Figure 11B–D**), as would be expected from observations in previous years. Through the intensive bottle sampling, proxy development, and particle characterizations conducted during

Table 5. Synthesis working groups. DOI: https://doi.org/10.1525/elementa.2020.00107.t5

Synthesis Working Group	Goals of the SWG	SWG Leads
1: Export pathways	Quantify the five export pathways illustrated in the wiring diagram (Figure 2)	Estapa (UMaine), Stamieszkin (VIMS)
2: Food web	Compile stock and rate measurements to assemble the wiring diagram for both the euphotic and mesopelagic zones	Rynearson (URI), Gifford (UNC), McNair (URI), Lerch (URI), Fox (OSU)
3: Optics	Validate optical proxies to biogeochemical stocks and rates	Graff (OSU), Nelson (UCSB), Kramer (UCSB)
4: Time and space	Attribute the sources of variability in physical and biogeochemical fields to space and/or time	Thompson (CalTech), Erickson (NASA GSFC), Omand (URI)
5: Biogeochemical budgets	Assess the biogeochemical budgets	Nicholson (WHOI), Roca Martî (WHOI), Stephens (UCSB)

the cruise period, the variation in bio-optical properties observed by the autonomous platforms will be used to understand the seasonal changes in export for the year(s) following the cruise. Additional observations drawn from other sources, including satellite remote sensing, OOI Station Papa assets, the BCG float array, and the Line P program, will be used to expand understanding of export processes over an even broader range of biological and physical variability.

Next steps

We have presented background and goals of the EXPORTS program, highlighted the logistics and operations of the 2018 field campaign in the NE Pacific, and provided a synthesis of oceanographic context during the cruise to set the stage for manuscripts on various core data sets for this special collection in *Elementa*. Documentation of the accomplishments of the EXPORTS team during the 2018 NE Pacific field campaign, accompanied by the online availability of likely one of the most comprehensive coupled biogeochemical-ecological-oceanographic data sets collected to date (https://sites.google.com/view/oceanexports/home; EXPORTS Science Team, 2020), is critical for NASA's implementation of an EXPORTS Phase 2 program (see timeline in **Figure 3**). The papers in this special collection of *Elementa* are a first step towards answering the EXPORTS science questions and delivering on its promise to develop a predictive understanding of the biological pump.

As the first results focused on project level questions are published, the EXPORTS science team has been synthesizing their findings across projects. Over the past 2 years, five Synthesis Working Groups (SWGs) have been meeting monthly. The SWGs are focused on quantifying and understanding the following: (1) export pathways, (2) food web processes, (3) optical proxies, (4) time and space variability, and (5) BGC budgets (**Table 5**). Some of the early results from the SWGs have been presented here. For example, the mixed-layer water mass analysis and air–sea flux analyses (**Figures 15** and **16**) were the result of SWG 4. Other working groups have been assembling the flows of carbon through upper ocean and mesopelagic food webs (SWG 2) or assessing biogeochemical carbon budgets (SWG 5). These activities are critical for answering the EXPORTS science questions, but also help to ensure the quality and consistency among the entire measurement suite. The latter is especially critical given that many of the parameters sampled were either measured on different platforms or using different approaches or both.

With the global COVID-19 pandemic continuing at the time of submission of this manuscript, our view into the future was cloudy at best. The North Pacific experiment is only part of the EXPORTS story—an "endmember" in the Ez-ratio and T_{100} space illustrated in **Figure 1**. While the North Atlantic experiment is needed to balance our understanding of how NPP carbon flows through the oceans of today and those of tomorrow, the breadth and complexity of the North Pacific EXPORTS deployment is destined to fuel new discoveries and pave the path for similar programs around the world. As this manuscript reached acceptance (May 2021), we can report that the North Atlantic EXPORTS experiment near the Porcupine Abyssal Plains Sustained Observatory (PAP-SO) site (https://projects.noc.ac.uk/pap/) in the northeast Atlantic Ocean is underway.

In July 2019, a group of researchers gathered in Southampton, UK, to form the Joint Exploration of the Twilight Zone Ocean Network (JETZON; https://jetzon.org). JETZON brought together scientists from 13 international projects tackling aspects of the role and function of the mesopelagic region of the oceans, the so-called twilight zone. A major goal of JETZON is to coordinate national studies of the biological carbon pump to optimize the understanding that these individual programs can provide by working together (Martin et al., 2020). To truly develop a predictive understanding of the fate of ocean NPP and its roles in the ocean carbon cycle, data from oceans around the world need to be synthesized. The hope is that by working together we can collect the global data sets needed to quantify the processes driving the ocean's biological pump and thus develop models that predict the present and future impacts of ocean ecological processes on the global carbon cycle.

Data accessibility statement

Data sets used in this paper can be found at: EXPORTS, 2018, SeaBASS, DOI: http://dx.doi.org/10.5067/SeaBASS/EXPORTS/DATA001. EXPORTS, 2018, BCO-DMO, https://www.bco-dmo.org/program/757397 (individual doi listed).

Acknowledgments

The EXPORTS Science Team would like to acknowledge support from the NASA Ocean Biology and Biogeochemistry program and the National Science Foundation Biological and Chemical Oceanography programs. Thanks go to the captains and crews of the R/Vs *Revelle* and *Ride* and to the Ship Operations staff of the Scripps Institution of Oceanography. We are grateful for the support of our collaborators from Canadian Line P program and OOI. Special thanks to Paula Bontempi (formally NASA HQ), Laura Lorenzoni (NASA HQ), Mike Sieracki (NSF BIO-OCE), and Quincy Allison and his team (NASA AMES) for their vision and support throughout the development and implementation of the EXPORTS field campaign.

Funding

DAS, NN, KB, EF, SK, AB, AM, UP: NASA 80NSSC17K0692. MJB, EB, JG, LG, KH, LKB, JF, NH: NASA 80NSSC17K0568. KB, CBN, LR, MRM: NASA 80NSSC17K0555. CC, DH, BS: NASA 80NSSC18K0437. HC: NSF 1830016. BP, KDS: NSF 1829425. ME, KB, CD, MO: NASA 80NSSC17K0662. AF: NSF 1756932. BJ, KB, MB, SB, SC: NSF 1756442. PH, OM, JML: NSF 1829614. CL, ED, DN, MO, MJP, AT, ZN, ST: NASA 80NSSC17K0663. AM, NC, SG, WT, AN, WG: NASA 80NSSC17K0552. SMD, TR, HM, FM: NASA 80NSSC17K0716. CR, HS: NASA 80NSSC17K0700. AS, PB: NASA 80NSSC18K1431. DS, AM, KS NASA 80NS SC17K0654. BVM: NSF 1756254. XZ, DG, LG, YH: NASA 80NSSC17K0656 and 80NSSC20K0350.

Competing interests

The authors have declared that no competing interests exist.

Author contributions

Contributed to conception and design: DAS, IC, JRG, CL, NN, MJP, ISR, DKS, KB, RH, AJF, DN, MMO, AT.

Contributed to acquisition of data: All.

Contributed to analysis and interpretation of data: DAS, IC, JRG, CL, NN, MJP, ISR, DKS, KB, RH, AJF, DN, MMO, MR, AT.

Drafted and/or revised the article: All.

Approved the submitted version for publication: All.

References

Balch, W, Evans, R, Brown, J, Feldman, G, McClain, C, Esaias, W. 1992. The remote sensing of ocean primary productivity: Use of a new data compilation to test satellite algorithms. *Journal of Geophysical Research: Oceans* **97**(C2): 2279–2293. DOI: http://dx.doi.org/10.1029/91jc02843.

Behrenfeld, MJ, Boss, E, Siegel, DA, Shea, DM. 2005. Carbon-based ocean productivity and phytoplankton physiology from space. *Global Biogeochemical Cycles* **19**(1): GB1006. DOI: http://dx.doi.org/10.1029/2004GB002299.

Behrenfeld, MJ, Falkowski, PG. 1997. Photosynthetic rates derived from satellite-based chlorophyll concentration. *Limnology and Oceanography* **42**(1): 1–20. DOI: http://dx.doi.org/10.4319/lo.1997.42.1.0001.

Behrenfeld, MJ, O'Malley, RT, Boss, ES, Westberry, TK, Graff, JR, Halsey, K, Kimberly, H, Milligan, AJ, Siegel, DA, Brown, MB. 2016. Revaluating ocean warming impacts on global phytoplankton. *Nature Climate Change* **6**(3): 323.

Behrenfeld, MJ, O'Malley, RT, Siegel, DA, McClain, CR, Sarmiento, JL, Feldman, GC, Milligan, AJ, Falkowski, PG, Letelier, RM, Boss, ES. 2006. Climate-driven trends in contemporary ocean productivity. *Nature* **444**: 752–755. DOI: http://dx.doi.org/10.1038/nature05317.

Bif, MB, Siqueira, L, Hansell, DA. 2019. Warm events induce loss of resilience in organic carbon production in the Northeast Pacific Ocean. *Global Biogeochem Cycles* **33**(9): 1174–1186. DOI: http://dx.doi.org/10.1029/2019gb006327.

Bisson, K, Siegel, DA, DeVries, T. 2020. Diagnosing mechanisms of ocean carbon export in a satellite-based food web model. *Frontiers in Marine Science* **7**(505). DOI: http://dx.doi.org/10.3389/fmars.2020.00505.

Bisson, KM, Siegel, DA, DeVries, T, Cael, BB, Buesseler, KO. 2018. How data set characteristics influence ocean carbon export models. *Global Biogeochem Cycles* **32**(9): 1312–1328. DOI: http://dx.doi.org/10.1029/2018gb005934.

Boss, E, Picheral, M, Leeuw, T, Chase, A, Karsenti, E, Gorsky, G, Taylor, L, Slade, W, Ras, J, Claustre, H. 2013. The characteristics of particulate absorption, scattering and attenuation coefficients in the surface ocean; Contribution of the Tara Oceans expedition. *Methods in Oceanography* **7**: 52–62. DOI: http://dx.doi.org/10.1016/j.mio.2013.11.002.

Boyd, P, Muggli, D, Varela, D, Goldblatt, R, Chretien, R, Orians, KJ, Harrison, PJ. 1996. In vitro iron enrichment experiments in the NE subarctic Pacific. *Marine Ecology Progress Series* **136**: 179–193.

Boyd, PW, Claustre, H, Levy, M, Siegel, DA, Weber, T. 2019. Multi-faceted particle pumps drive carbon sequestration in the ocean. *Nature* **568**(7752): 327–335. DOI: http://dx.doi.org/10.1038/s41586-019-1098-2.

Boyd, PW, Harrison, PJ, Johnson, BD. 1999. The Joint Global Ocean Flux Study (Canada) in the NE subarctic Pacific. *Deep Sea Research Part II* **46**(11): 2345–2350. DOI: http://dx.doi.org/10.1016/S0967-0645(99)00066-1.

Boyd, PW, Law, CS, Wong, CS, Nojiri, Y, Tsuda, A, Levasseur, M, Takeda, S, Rivkin, R, Harrison, PJ, Strzepek, R, Gower, J, McKay, M, Abraham, E, Arychuk, M, Barwell-Clarke, J, Crawford, W, Crawford, D, Hale, M, Harada, K, Johnson, K, Kiyosawa, H, Kudo, I, Marchetti, A, Miller, W,

Needoba, J, Nishioka, J, Ogawa, H, Page, J, Robert, M, Saito, H, Sastri, A, Sherry, N, Soutar, T, Sutherland, N, Taira, Y, Whitney, F, Wong, S-KE, Yoshimura, T. 2004. The decline and fate of an iron-induced subarctic phytoplankton bloom. *Nature* **428**(6982): 549–553. DOI: http://dx.doi.org/10.1038/nature02437.

Buesseler, KO, Benitez-Nelson, CR, Roca-Martí, M, Wyatt, AM, Resplandy, L, Clevenger, SJ, Drysdale, JA, Estapa, ML, Pike, S, Umhau, BP. 2020a. High resolution spatial and temporal measurements of particulate organic carbon flux using thorium-234 in the NE Pacific Ocean during the EXPORTS Program. *Elementa: Science of the Anthropocene* **8**(1): 030. DOI: http://dx.doi.org/10.1525/elementa.030.

Buesseler, KO, Boyd, PW. 2009. Shedding light on processes that control particle export and flux attenuation in the twilight zone of the open ocean. *Limnology and Oceanography* **54**(4): 1210–1232. DOI: http://dx.doi.org/10.4319/lo.2009.54.4.1210.

Buesseler, KO, Boyd, PW, Black, EE, Siegel, DA. 2020b. Metrics that matter for assessing the ocean biological carbon pump. *Proceedings of the National Academy of Sciences* **117**(18): 9679–9687. DOI: http://dx.doi.org/10.1073/pnas.1918114117.

Bushinsky, SM, Emerson, S. 2015. Marine biological production from in situ oxygen measurements on a profiling float in the subarctic Pacific Ocean. *Global Biogeochem Cycles* **29**(12): 2050–2060. DOI: http://dx.doi.org/10.1002/2015gb005251.

Campbell, J, Antoine, D, Armstrong, R, Arrigo, K, Balch, W, Barber, R, Behrenfeld, M, Bidigare, R, Bishop, J, Carr, M-E, Esaias, W, Falkowski, P, Hoepffner, N, Iverson, R, Kiefer, D, Lohrenz, S, Marra, J, Morel, A, Ryan, J, Vedernikov, V, Waters, K, Yentsch, C, Yoder, J. 2002. Comparison of algorithms for estimating ocean primary production from surface chlorophyll, temperature, and irradiance. *Global Biogeochem Cycles* **16**(3): 1035. DOI: http://dx.doi.org/10.1029/2001gb001444.

Cetinić, I, Perry, MJ, Briggs, NT, Kallin, E, D'Asaro, EA, Lee, CM. 2012. Particulate organic carbon and inherent optical properties during 2008 North Atlantic Bloom Experiment. *Journal of Geophysical Research-Oceans* **117**(C6). DOI: http://dx.doi.org/10.1029/2011jc007771.

Charette, MA, Moran, SB, Bishop, JK. 1999. ^{234}Th as a tracer of particulate organic carbon export in the subarctic northeast Pacific Ocean. *Deep Sea Research Part II: Topical Studies in Oceanography* **46**(11–12): 2833–2861.

Chelton, DB, Schlax, MG, Samelson, RM. 2011. Global observations of nonlinear mesoscale eddies. *Progress in Oceanography* **91**(2): 167–216. DOI: http://dx.doi.org/10.1016/j.pocean.2011.01.002.

Chelton, DB, Schlax, MG, Samelson, RM, de Szoeke, RA. 2007. Global observations of large oceanic eddies. *Geophysical Research Letters* **34**(15). DOI: http://dx.doi.org/10.1029/2007gl030812.

Cummins, PF, Freeland, HJ. 2007. Variability of the North Pacific Current and its bifurcation. *Progress in Oceanography* **75**(2): 253–265. DOI: http://dx.doi.org/10.1016/j.pocean.2007.08.006.

D'Asaro, EA. 2003. Performance of autonomous Lagrangian floats. *Journal of Atmospheric and Oceanic Technology* **20**(6): 896–911. DOI: http://dx.doi.org/10.1175/1520-0426(2003)020<0896:poalf>2.0.co;2.

D'Asaro, EA, Eriksen, CC, Levine, MD, Paulson, CA, Niiler, P, Van Meurs, P. 1995. Upper-ocean inertial currents forced by a strong storm. Part I: Data and comparisons with linear theory. *Journal of Physical Oceanography* **25**(11): 2909–2936. DOI: http://dx.doi.org/10.1175/1520-0485(1995)025<2909:uoicfb>2.0.co;2.

Davis, R, DeSzoeke, R, Halpern, D, Niiler, P. 1981. Variability in the upper ocean during MILE. Part I: The heat and momentum balances. *Deep Sea Research Part A. Oceanographic Research Papers* **28**(12): 1427–1451.

Denman, KL, Miyake, M. 1973. Upper layer modification at Ocean Station Papa: Observations and simulation. *Journal of Physical Oceanography* **3**(2): 185–196. DOI: http://dx.doi.org/10.1175/1520-0485(1973)003<0185:ulmaos>2.0.co;2.

DeVries, T, Le Quéré, C, Andrews, O, Berthet, S, Hauck, J, Ilyina, T, Landschützer, P, Lenton, A, Lima, ID, Nowicki, M, Schwinger, J, Séférian, R. 2019. Decadal trends in the ocean carbon sink. *Proceedings of the National Academy of Sciences* **116**(24): 11646–11651. DOI: http://dx.doi.org/10.1073/pnas.1900371116.

Eriksen, CC, Osse, TJ, Light, RD, Wen, T, Lehman, TW, Sabin, PL, Ballard, JW, Chiodi, AM. 2001. Seaglider: A long-range autonomous underwater vehicle for oceanographic research. *IEEE Journal of Oceanic Engineering* **26**(4): 424–436.

EXPORTS Science Definition Team. 2016. EXPORTS implementation plan. Available at https://oceanexports.org/docs_implementation_plan.html.

EXPORTS Science Team. 2020. *EXPORTS measurements and protocols for the NE pacific campaign*. Greenbelt, MD: NASA Goddard Space Flight Center. DOI: https://sites.google.com/view/oceanexports/home.

EXPORTS Writing Team. 2015. *EXport Processes in the Ocean from RemoTe Sensing (EXPORTS): A science plan for a NASA field campaign*. Available at https://oceanexports.org/documents/EXPORTS_Science_Plan_May18_2015_final.pdf.

Freeland, H. 2007. A short history of Ocean Station Papa and Line P. *Progress in Oceanography* **75**(2): 120–125. DOI: http://dx.doi.org/10.1016/j.pocean.2007.08.005.

Freeland, HJ, Cummins, PF. 2005. Argo: A new tool for environmental monitoring and assessment of the world's oceans, an example from the N.E. Pacific. *Progress in Oceanography* **64**(1): 31–44. DOI: http://dx.doi.org/10.1016/j.pocean.2004.11.002.

Friedlingstein, P, Jones, MW, O'Sullivan, M, Andrew, RM, Hauck, J, Peters, GP, Peters, W, Pongratz, J,

Sitch, S, Le Quéré, C, Bakker, DCE, Canadell, JG, Ciais, P, Jackson, RB, Anthoni, P, Barbero, L, Bastos, A, Bastrikov, V, Becker, M, Bopp, L, Buitenhuis, E, Chandra, N, Chevallier, F, Chini, LP, Currie, KI, Feely, RA, Gehlen, M, Gilfillan, D, Gkritzalis, T, Goll, DS, Gruber, N, Gutekunst, S, Harris, I, Haverd, V, Houghton, RA, Hurtt, G, Ilyina, T, Jain, AK, Joetzjer, E, Kaplan, JO, Kato, E, Klein Goldewijk, K, Korsbakken, JI, Landschützer, P, Lauvset, SK, Lefèvre, N, Lenton, A, Lienert, S, Lombardozzi, D, Marland, G, McGuire, PC, Melton, JR, Metzl, N, Munro, DR, Nabel, JEMS, Nakaoka, S-I, Neill, C, Omar, AM, Ono, T, Peregon, A, Pierrot, D, Poulter, B, Rehder, G, Resplandy, L, Robertson, E, Rödenbeck, C, Séférian, R, Schwinger, J, Smith, N, Tans, PP, Tian, H, Tilbrook, B, Tubiello, FN, van der Werf, GR, Wiltshire, AJ, Zaehle, S. 2019. Global Carbon Budget 2019. *Earth System Science Data* **11**(4): 1783–1838. DOI: http://dx.doi.org/10.5194/essd-11-1783-2019.

Graff, JR, Westberry, TK, Milligan, AJ, Brown, MB, Dall'Olmo, G, van Dongen-Vogels, V, Reifel, KM, Behrenfeld, MJ. 2015. Analytical phytoplankton carbon measurements spanning diverse ecosystems. *Deep Sea Research Part I: Oceanographic Research Papers* **102**: 16–25.

Haskell, WZ, Fassbender, AJ, Long, JS, Plant, JN. 2020. Annual net community production of particulate and dissolved organic carbon from a decade of biogeochemical profiling float observations in the Northeast Pacific. *Global Biogeochem Cycles* **34**. DOI: http://dx.doi.org//10.1029/2020GB006599.

Jackson, JM, Myers, PG, Ianson, D. 2006. An examination of advection in the northeast Pacific Ocean, 2001–2005. *Geophysical Research Letters* **33**(15). DOI: http://dx.doi.org/10.1029/2006gl026278.

Kramer, SJ, Siegel, DA. 2019. How can phytoplankton pigments be best used to characterize surface ocean phytoplankton groups for ocean color remote sensing algorithms?*Journal of Geophysical Research: Oceans* **124**(11): 7557–7574. DOI: http://dx.doi.org/10.1029/2019jc015604.

Kwon, EY, Primeau, F, Sarmiento, JL. 2009. The impact of remineralization depth on the air–sea carbon balance. *Nature Geoscience* **2**(9): 630–635. DOI: http://dx.doi.org/10.1038/ngeo612.

Large, WG, McWilliams, JC, Doney, SC. 1994. Oceanic vertical mixing: A review and a model with a nonlocal boundary layer parameterization. *Reviews in Geophysics* **32**(4): 363–403. DOI: http://dx.doi.org/10.1029/94rg01872.

Martin, A, Boyd, P, Buesseler, K, Cetinic, I, Claustre, H, Giering, S, Henson, S, Irigoien, X, Kriest, I, Memery, L, Robinson, C, Saba, G, Sanders, R, Siegel, D, Villa-Alfageme, M, Guidi, L. 2020. The oceans' twilight zone must be studied now, before it is too late. *Nature* **580**: 26–28.

Martin, JH, Fitzwater, SE. 1988. Iron deficiency limits phytoplankton growth in the north-east Pacific subarctic. *Nature* **331**(6154): 341–343. DOI: http://dx.doi.org/10.1038/331341a0.

Martin, JH, Gordon, RM, Fitzwater, S, Broenkow, WW. 1989. Vertex: Phytoplankton/iron studies in the Gulf of Alaska. *Deep Sea Research Part A. Oceanographic Research Papers* **36**(5): 649–680. DOI: http://dx.doi.org/10.1016/0198-0149(89)90144-1.

Measures, CI, Landing, WM, Brown, MT, Buck, CS. 2008. A commercially available rosette system for trace metal–clean sampling. *Limnology and Oceanography Methods* **6**(9): 384–394. DOI: http://dx.doi.org/10.4319/lom.2008.6.384.

Mellet, T, Buck, KN. 2020. Spatial and temporal variability of trace metals (Fe, Cu, Mn, Zn, Co, Ni, Cd, Pb), iron and copper speciation, and electroactive Fe-binding humic substances in surface waters of the eastern Gulf of Mexico. *Marine Chemistry* **277**. DOI: http://dx.doi.org/10.1016/j.marchem.2020.103891.

Mellor, GL, Durbin, PA. 1975. The structure and dynamics of the ocean surface mixed layer. *Journal of Physical Oceanography* **5**(4): 718–728. DOI: http://dx.doi.org/10.1175/1520-0485(1975)005<0718:tsadot>2.0.co;2.

Miller, CB, Frost, BW, Wheeler, PA, Landry, MR, Welschmeyer, N, Powell, T. 1991. Ecological dynamics in the subarctic Pacific, a possibly iron-limited ecosystem. *Limnology and Oceanography* **36**(8): 1600–1615. DOI: http://dx.doi.org/10.4319/lo.1991.36.8.1600.

Nelson, NB, Siegel, DA. 2013. The global distribution and dynamics of chromophoric dissolved organic matter. *Annual Review of Marine Science* **5**(1): 447–476. DOI: http://dx.doi.org/10.1146/annurev-marine-120710-100751.

Parsons, TR, Lalli, CM. 1988. Comparative oceanic ecology of the plankton communities of the subarctic Atlantic and Pacific oceans. *Oceanography and Marine Biology: An Annual Review* **26**: 317–359.

Pelland, NA, Eriksen, CC, Cronin, MF. 2016. Seaglider surveys at Ocean Station Papa: Circulation and water mass properties in a meander of the North Pacific Current. *Journal of Geophysical Research: Oceans* **121**(9): 6816–6846. DOI: http://dx.doi.org/10.1002/2016jc011920.

Pelland, NA, Eriksen, CC, Cronin, MF. 2017. Seaglider surveys at Ocean Station Papa: Diagnosis of upper-ocean heat and salt balances using least squares with inequality constraints. *Journal of Geophysical Research: Oceans* **122**(6): 5140–5168. DOI: http://dx.doi.org/10.1002/2017jc012821.

Pelland, NA, Eriksen, CC, Emerson, SR, Cronin, MF. 2018. Seaglider surveys at Ocean Station Papa: Oxygen kinematics and upper-ocean metabolism. *Journal of Geophysical Research: Oceans* **123**(9): 6408–6427. DOI: http://dx.doi.org/10.1029/2018JC014091.

Plant, JN, Johnson, KS, Sakamoto, CM, Jannasch, HW, Coletti, LJ, Riser, S, Swift, DD. 2016. Net community production at Ocean Station Papa observed with

nitrate and oxygen sensors on profiling floats. *Global Biogeochemical Cycles* **30**(6): 859–879. DOI: http://dx.doi.org/10.1002/2015gb005349.

Price, JF, Weller, RA, Pinkel, R. 1986. Diurnal cycling: Observations and models of the upper ocean response to diurnal heating, cooling, and wind mixing. *Journal of Geophysical Research: Oceans* **91**(C7): 8411–8427. DOI: http://dx.doi.org/10.1029/JC091iC07p08411.

Rainville, L, Pinkel, R. 2001. Wirewalker: An autonomous wave-powered vertical profiler. *Journal of Atmospheric and Oceanic Technology* **18**(6): 1048–1051. DOI: http://dx.doi.org/10.1175/1520-0426(2001)018<1048:waawpv>2.0.co;2.

Resplandy, L, Lévy, M, McGillicuddy Jr., DJ. 2019. Effects of eddy-driven subduction on ocean biological carbon pump. *Global Biogeochemical Cycles* **33**(8): 1071–1084. DOI: http://dx.doi.org/10.1029/2018gb006125.

Rousseaux, CS, Gregg, WW. 2017. Forecasting ocean chlorophyll in the Equatorial Pacific. *Frontiers in Marine Science* **4**(236). DOI: http://dx.doi.org/10.3389/fmars.2017.00236.

Schallenberg, C, Ross, ARS, Davidson, AB, Stewart, GM, Cullen, JT. 2017. Temporal variability of dissolved iron species in the mesopelagic zone at Ocean Station PAPA. *Journal of Marine Systems* **172**: 128–136. DOI: http://dx.doi.org/10.1016/j.jmarsys.2017.03.006.

Siegel, DA, Buesseler, KO, Behrenfeld, MJ, Benitez-Nelson, CR, Boss, E, Brzezinski, M, Burd, A, Carlson, CA, D'Asaro, EA, Doney, SC, Perry, MJ, Stanley, RHR, Steinberg, DK. 2016. Prediction of the export and fate of global ocean net primary production: The EXPORTS Science Plan. *Frontiers in Marine Science* **3**. DOI: http://dx.doi.org/10.3389/fmars.2016.00022.

Silsbe, GM, Behrenfeld, MJ, Halsey, KH, Milligan, AJ, Westberry, TK. 2016. The CAFE model: A net production model for global ocean phytoplankton. *Global Biogeochemical Cycles* **30**(12): 1756–1777. DOI: http://dx.doi.org/10.1002/2016gb005521.

Stramski, D, Kiefer, DA. 1991. Light scattering by microorganisms in the open ocean. *Progress in Oceanography* **28**: 343–383.

Tabata, S. 1965. Variability of oceanic conditions at Ocean Station P in the northeast Pacific Ocean. *Transactions of the Royal Society of Canada* **4**(3): 367–418.

Werdell, PJ, Behrenfeld, MJ, Bontempi, PS, Boss, E, Cairns, B, Davis, GT, Franz, BA, Gliese, UB, Gorman, ET, Hasekamp, O, Knobelspiesse, KD, Mannino, A, Martins, JV, McClain, CR, Meister, G, Remer, LA. 2019. The Plankton, Aerosol, Cloud, Ocean Ecosystem mission: Status, science, advances. *Bulletin of the American Meteorological Society* **100**(9): 1775–1794. DOI: http://dx.doi.org/10.1175/bams-d-18-0056.1.

Westberry, T, Behrenfeld, MJ, Siegel, DA, Boss, E. 2008. Carbon-based primary productivity modeling with vertically resolved photoacclimation. *Global Biogeochemical Cycles* **22**(2). DOI: http://dx.doi.org/10.1029/2007GB003078.

Whitney, FA, Crawford, WR, Harrison, PJ. 2005. Physical processes that enhance nutrient transport and primary productivity in the coastal and open ocean of the subarctic NE Pacific. *Deep Sea Research Part II: Oceanographic Research Papers* **52**(5): 681–706. DOI: http://dx.doi.org/10.1016/j.dsr2.2004.12.023.

Whitney, FA, Freeland, HJ. 1999. Variability in upper-ocean water properties in the NE Pacific Ocean. *Deep Sea Research Part II: Oceanographic Research Papers* **46**(11): 2351–2370. DOI: http://dx.doi.org/10.1016/S0967-0645(99)00067-3.

Wong, C, Whitney, F, Iseki, K, Page, J, Zeng, J. 1995. Analysis of trends in primary productivity and chlorophyll-a over two decades at Ocean Station P (50 N, 145 W) in the subarctic northeast Pacific Ocean. *Canadian Journal of Fisheries and Aquatic Sciences* **121**: 107–117.

Xu, C, Shang, X-D, Huang, RX. 2014. Horizontal eddy energy flux in the world oceans diagnosed from altimetry data. *Scientific Reports* **4**(1): 5316. DOI: http://dx.doi.org/10.1038/srep05316.

Yang, B, Emerson, SR, Peña, MA. 2018. The effect of the 2013–2016 high temperature anomaly in the subarctic Northeast Pacific (the "Blob") on net community production. *Biogeosciences* **15**(21): 6747–6759. DOI: http://dx.doi.org/10.5194/bg-15-6747-2018.

Zhang, X, Hu, L, Xiong, Y, Huot, Y, Gray, D. 2020. Experimental estimates of optical backscattering associated with submicron particles in clear oceanic waters. *Geophysical Research Letters* **47**(4): e2020GL087100. DOI: http://dx.doi.org/10.1029/2020gl087100.

How to cite this article: Siegel, DA, Cetinić, I, Graff, JR, Lee, CM, Nelson, N, Perry, MJ, Ramos, IS, Steinberg, DK, Buesseler, K, Hamme, R, Fassbender, AJ, Nicholson, D, Omand, MM, Robert, M, Thompson, A, Amaral, V, Behrenfeld, M, Benitez-Nelson, C, Bisson, K, Boss, E, Boyd, PW, Brzezinski, M, Buck, K, Burd, A, Burns, S, Caprara, S, Carlson, C, Cassar, N, Close, H, D'Asaro, E, Durkin, C, Erickson, Z, Estapa, ML, Fields, E, Fox, J, Freeman, S, Gifford, S, Gong, W, Gray, D, Guidi, L, Haëntjens, N, Halsey, K, Huot, Y, Hansell, D, Jenkins, B, Karp-Boss, L, Kramer, S, Lam, P, Lee, JM, Maas, A, Marchal, O, Marchetti, A, McDonnell, A, McNair, H, Menden-Deuer, S, Morison, F, Niebergall, AK, Passow, U, Popp, B, Potvin, G, Resplandy, L, Roca-Martí, M, Roesler, C, Rynearson, T, Traylor, S, Santoro, A, Seraphin, KD, Sosik, HM, Stamieszkin, K, Stephens, B, Tang, W, Van Mooy, B, Xiong, Y, Zhang, X. 2021. An operational overview of the EXport Processes in the Ocean from RemoTe Sensing (EXPORTS) Northeast Pacific field deployment. *Elementa: Science of the Anthropocene* 9(1). DOI: https://doi.org/10.1525/elementa.2020.00107

Domain Editor-in-Chief: Jody W. Deming, University of Washington, Seattle, WA, USA

Knowledge Domain: Ocean Science

Part of an Elementa Special Feature: Accomplishments from the EXport Processes in the Ocean from RemoTe Sensing (EXPORTS) Field Campaign to the Northeast Pacific Ocean

Published: July 7, 2021 **Accepted:** May 24, 2021 **Submitted:** July 20, 2020

ELEMENTA Science of the Anthropocene

Elem Sci Anth is a peer-reviewed open access journal published by University of California Press.

OPEN ACCESS